Available online at www.sciencedirect.com
ScienceDirect
Trans. Nonferrous Met. Soc. China 31(2021) 3228−3254
Transactions of Nonferrous Metals Society of China
www.tnmsc.cn

Corrosion behavior of Mg−Li alloys: A review

Xiao-chun MA[1], Si-yuan JIN[1], Rui-zhi WU[1,2], Jia-xiu WANG[1], Gui-xiang WANG[1], Boris KRIT[3], Sergey BETSOFEN[3]

1. Key Laboratory of Superlight Materials & Surface Technology, Ministry of Education, Harbin Engineering University, Harbin 150001, China;
2. College of Science, Heihe University, Heihe 164300, China;
3. Moscow Aviation Institute, National Research University, Moscow 125993, Russia

Received 29 September 2021; accepted 2 November 2021

Abstract: It has been known that the lack of excellent corrosion resistance is the key problem restricting the wide application of Mg−Li alloys. Based on a quantity of literature about corrosion behavior of Mg−Li alloys, this review elaborates the factors affecting the corrosion behavior of Mg−Li alloys and the processing methods for improving corrosion resistance. The corrosion characteristics of Mg−Li alloys are described firstly. Then, it is explained that the grain size, orientation, second phase, and surface film strongly influence corrosion performance, which can be tailored by alloying, plastic deformation, and heat treatment. Further in-depth discussion about the corrosion mechanisms for Mg−Li alloys was also presented. Finally, important points of improving corrosion resistance are suggested.
Key words: Mg−Li alloy; corrosion behavior; microstructure; surface film; alloying; plastic deformation; heat treatment

1 Introduction

Magnesium−lithium (Mg−Li) alloys, as the lightest metal engineering material, have attracted extensive attention. In the early 20th century, the Mg−Li binary phase diagram was determined based on the phase structure transformation of Mg and Li found by TAMMAN [1]. Subsequently, some classic Mg−Li alloys were successfully manufactured, such as LAZ933 and LA141 in USA, MA18 and MA21 in Soviet Union [2]. Until the end of the 20th century, Japan and China began to study Mg−Li ultralight alloys. In recent years, due to the excellent ultralight characteristics of Mg−Li alloys and the urgent light-weight requirement from industry, the research and application about Mg−Li alloys are becoming hot issue. And there are many outstanding achievements in the preparation, processing and surface treatment of Mg−Li alloys.

Since weight reduction is a requisite for increasing fuel efficiency and reducing emissions, Mg−Li alloys with a density of only 1.30−1.65 g/cm^3 are ideal light-weight alloys [3], which have great prospects in military [4], aerospace [5] and automobile [6], and continue to develop in 3C industry, biomedicine, electrochemical power supply and other civilian fields [7]. This is based on the advantages of Mg−Li alloys in terms of high specific strength [8] and specific stiffness [9], low anisotropy [10], excellent electromagnetic shielding [11,12] and damping properties [13], and non-toxicity and good biocompatibility [14]. The addition of Li reduces the critical shear stress and c/a ratio of Mg crystal so as to improve the formability of the alloys [4], especially the low-temperature toughness [15]. Depending on the content of Li, Mg−Li alloys present different crystal structures, that is, when the content of Li is less than 5.7 wt.%, the solid solution of Li in Mg (α-Mg)

Corresponding author: Rui-zhi WU, Tel/Fax: +86-451-82569890, E-mail: rzwu@hrbeu.edu.cn;
Gui-xiang WANG, Tel/Fax: +86-451-82569890, E-mail: wangguixiang@hrbeu.edu.cn
DOI: 10.1016/S1003-6326(21)65728-X

is hcp structure; when the content of Li is higher than 10.3 wt.%, the solid solution of Mg in Li (β-Li) with bcc structure is formed, and the addition of 5.7−10.3 wt.% Li promotes the formation of a unique dual-phase structure (α-Mg+β-Li) in Mg−Li alloys [3].

Figure 1 illustrates the dependence of Mg−Li alloys on the processing, microstructure, properties and applications. So far, there still exist challenges in the practical engineering application of Mg−Li alloys, among which the poor corrosion resistance is one of the most frequently stated problems and constraints [16]. A large quantity of literature has reported the corrosion and protection of Mg−Li alloys. On the one hand, the effects of microstructure on corrosion behavior of Mg−Li alloys have been discussed through alloying [17], heat treatment [18], mechanical deformation [19] and other processing methods. On the other hand, various surface treatments have been applied to improving the corrosion resistance of Mg−Li alloys, such as plating [20], anodizing [21], and laser coating [22]. SUN et al [23] reported researches on corrosion behavior of α-phase, (α+β)-phase and β-phase in Mg−Li alloys, respectively. WANG et al [24] summarized the corrosion research progress of Mg−Li alloys with different crystal structures as well as corrosion protective film on the surfaces. CAIN [25] detailed the microstructure, strengthening behavior and corrosion properties of β-phase Mg−Li alloys. However, not only different crystal structures have significant influence on the corrosion behavior, but also the grain, second phase and surface film are pivotal factors affecting the corrosion performance of Mg−Li alloys.

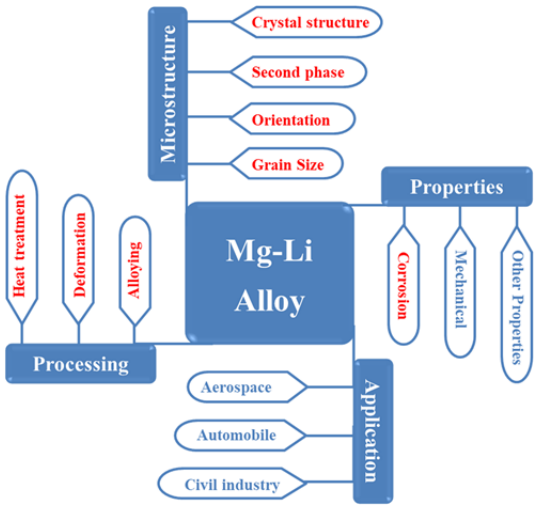

Fig. 1 Schematic graphic representation of Mg−Li alloys and its dependency on processing, properties and microstructure

Based on this, the review herein firstly carries out the brief description about the corrosion characteristics and corrosion process of Mg−Li alloys. This is followed by a summary of the aspects influencing corrosion behavior of Mg−Li alloys with an emphasis on microstructure, surface film, and the corresponding processing. This review contributes to deepening the understanding of the corrosion mechanism of Mg−Li alloys, aiming to provide a reference for the development of corrosion resistant Mg−Li alloys.

2 Corrosion characteristics of Mg−Li alloys

Mg is chemically active with a standard potential of −2.37 V, which is prone to produce oxides and hydroxides through chemical and electrochemical reactions in the atmosphere and seawater. The intrinsic corrosion rate of high-purity Mg as measured by weight-loss method is 0.3 mm/a in a NaCl solution. Other Mg alloys such as Mg−Al and Mg−Zn alloys typically have corrosion rates in NaCl solutions greater than the intrinsic corrosion rate of Mg of 0.3 mm/a, and the most corrosion rates are above 1 mm/a. The two exceptions of Mg alloys with a corrosion rate in a chloride solution of 0.1 mm/a are Mg−1.5Sr alloy and Mg−4Y−3Nd alloy. Li is a more active metal than Mg with a standard potential of −3.04 V, resulting in easier corrosion and severer erosion of Mg−Li alloys [26]. Recently, the lowest corrosion rate of the Mg−Li alloy is 0.8 mm/a measured by weight-loss method in 0.1 mol/L NaCl solutions and that is 10 mm/a in 3.5 wt.% NaCl solutions, which are substantially above the intrinsic corrosion rate of pure Mg but lower than those of most Mg alloys [6]. In general Mg alloys, the potentials of the alloying elements are more positive than those of Mg, forming second phases of the cathode to promote micro-galvanic corrosion of Mg anode. While in Mg−Li alloys, once Li dissolves preferentially, the remaining Mg will follow to sustain corrosion or even fall off, leading to the poor corrosion resistance.

Reacting with water and aggressive ions in aqueous solution, Mg evolves hydrogen at the cathode and dissolves at the anode, and the

corrosion process of Mg alloys is similar to aforementioned reactions, with some alloy elements simultaneously dissolving at the anode. Both Mg and Li are active metal elements dissolving in water, followed by the corrosion reaction processes of Mg−Li alloys shown in Reactions (1)–(6) [27]:

Cathode reaction:

$$2H_2O+2e^-\rightarrow H_2\uparrow+2OH^- \quad (1)$$

Anode reaction:

$$Mg\rightarrow Mg^{2+}+2e^- \quad (2)$$

$$Li\rightarrow Li^{+}+e^- \quad (3)$$

Formation of corrosion products:

$$Mg^{2+}+2OH^-\rightarrow Mg(OH)_2 \quad (4)$$

$$Li^{+}+OH^-\rightarrow LiOH \quad (5)$$

Total reaction:

$$Mg+2Li+4H_2O\rightarrow Mg(OH)_2+2LiOH+2H_2\uparrow \quad (6)$$

It should be noted that the anodic Reaction (2) describes the total reaction of anodic dissolution process, while there are several intermediate processes involving partially protective surface film, uni-positive Mg^+ ion, Mg hydride, cathodic catalytic activity and multiple different corrosion reaction mechanisms [28]. Considering the exposure of O_2 and CO_2 in the environment, the corrosion products will further react as follows:

$$2Mg^{2+}+O_2\rightarrow 2MgO \quad (7)$$

$$Mg(OH)_2+CO_2\rightarrow MgCO_3+H_2O \quad (8)$$

$$4Li^{+}+O_2\rightarrow 2Li_2O \quad (9)$$

$$2LiOH+CO_2\rightarrow Li_2CO_3 \quad (10)$$

Due to different Li contents, Mg−Li alloys exhibit distinct crystal structures, and both Li content and crystal structure play a vital role in the corrosion behavior of Mg−Li alloys, of which the effects in detail and research progress are summarized below. It has been shown that the characteristic of the corrosion behavior of Mg−Li alloy with time differs from that of traditional Mg alloys. HUANG et al [29] found that the corrosion rate of Mg−Li alloy is lower than that of pure Mg after 24 h immersion in 3.5 wt.% NaCl solution, and there are smaller and shallower corrosion pits on the surface of Mg−Li alloy, even though the corrosion resistance of pure Mg is better than that of Mg−Li alloy at the initial corrosion stage. By comparing the corrosion performance over time of dual-phase Mg−8.8Li alloy with that of AZ91D traditional Mg alloy, SONG et al [30] reached the same conclusion that AZ91D alloy is more corrosion resistant than Mg−8.8Li alloy proved by polarization curve and electrochemical impedance spectroscopy when just immersed in corrosive solution, while the mass loss rate of Mg−8.8Li alloy decreases and is less than that of AZ91D alloy with the extension of immersion time (after 48 h). It is caused by the higher activity of Li, resulting in rapid corrosion of Mg−8.8Li alloy at the beginning of immersion, and Al in AZ91D alloy can promote the surface passivation. The protective surface film of AZ91D is destroyed as the corrosion elongates, and the severe galvanic corrosion happens between Mg matrix and cathode second phase leading to forming deeper corrosion pits, while the Mg−8.8Li alloy gradually develops a more uniform general corrosion from pitting corrosion and filiform corrosion.

As for the corrosion mechanism of Mg−Li alloys, SONG et al [27] stated the occurrence and characteristic of filiform corrosion in Mg−8Li alloy. The corrosion damage occurs preferentially at the interface of α-Mg phase and β-Li phase, and then extends to the β phase due to higher activity. Figure 2(a) shows the schematic diagram of filiform corrosion on Mg−8Li alloy. In the occurrence of filiform corrosion, the filament tip is acidic with Mg dissolution reaction, and the filament tail is passivated by the corrosion product of $Mg(OH)_2$ and LiOH in alkaline environment. The addition of Li promotes the hydrogen evolution reaction at the cathode, correspondingly accelerating the propagation of the filament. Recent studies have indicated that, after the damage starts at the phase interface, the corrosion is prior to extend in α-Mg phase in the form of filiform characteristic, while it shows intergranular corrosion in β-Li phase [31]. XU et al [32] proved that the Li_2CO_3 film formed on the surface of Mg−Li alloy is dense and protective, which has a positive impact on the improvement of corrosion resistance. This is mainly because the standard enthalpy of Li_2CO_3 is low, where a low enthalpy of formation indicates the high chemical stability, and the value of PBR is about 1.27. Figure 2(b) demonstrates surface layer formation on hcp Mg and bcc Mg−Li alloys, and the formation of passivated Li_2CO_3 is due to the

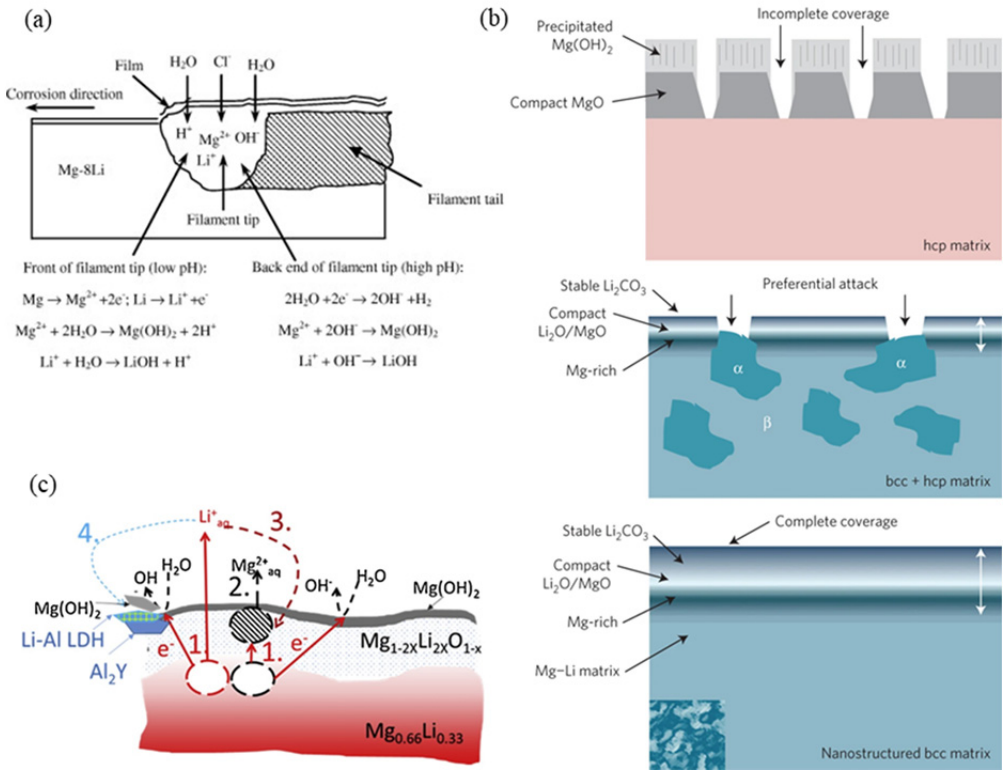

Fig. 2 Schematic diagrams of corrosion mechanism of Mg−Li alloys: (a) Sketch map of filiform corrosion on Mg−8Li alloy [27]; (b) Surface layer formation on hcp Mg and bcc Mg−Li after exposure to standard atmospheric conditions [32]; (c) Schematic representation of steps of aqueous corrosion of Mg−Li alloy [33]

homogeneous nanoscale microstructure in the Mg−Li−Al−Y−Zr alloy. Recently, YAN et al [33] have adopted a variety of in-situ analysis techniques to demonstrate the stability of Mg−Li alloy in water owing to generating Li-doped MgO film and Li−Al LDH and the Li-lean hcp Mg−Li phase under the oxide film as shown in Fig. 2(c).

In order to determine the corrosion rate and other corrosion parameters of Mg−Li alloy, and determine the relationship between corrosion behavior and microstructure, so as to further elaborate the corrosion mechanism, it is common practice to make use of a set of conventional methods, including gravimetric methods, hydrogen gas collection, visual inspection, optical and electron microscopy and electro-chemical measurements [24,25]. Recently, corrosion researches of Mg−Li alloys have benefited from the development of modern analytical techniques. It may be noted that in situ analysis is necessary to investigate corrosion in real time and on the exact location such as the initiation of corrosion and understand the dynamics of a corrosion process. The modern and in situ methods used in corrosion studies of Mg−Li alloys include scanning vibrating electrode technique (SVET), scanning Kelvin probe (SKP), SKP-force microscopy (SKPFM), atomic emission spectroelectrochemistry (AESEC) and secondary ion mass spectrometry (SIMS) [28,32,33].

3 Influencing factors for corrosion behavior of Mg−Li alloys

3.1 Li content

It is generally recognized that the Li content has a significant influence on the microstructure and properties of Mg−Li alloys. Different Li contents cause the formation of different solid solutions in the Mg−Li alloys, showing α-Mg (<5.7 wt.% Li), $\alpha+\beta$ (5.7−10.3 wt.% Li) and β-Li (>10.3 wt.% Li). Researches have commonly revealed that corrosion behavior of Mg−Li alloys is closely related to different crystal structures. However, the hcp and bcc crystal structures themselves do not seem to change the corrosion rate and corrosion type of the alloy, and it is Li content that affects the corrosion resistance of Mg−Li alloys.

Table 1 lists the corrosion rates of some Mg−Li alloys with different Li contents.

The electrochemical test results showed that the corrosion current density of Mg−Li alloys increases gradually after adding 4.5, 7.5 and 15 wt.% Li, respectively [45]. Among the Mg−(4.5, 7.5, 15)Li−Al−Zn alloys [34] and Mg−(1, 9, 15)Li−1Ca alloys [35], it is stated that a small amount

Table 1 Corrosion rates of some Mg−Li alloys with different Li contents

Alloy	State	Li content/ wt.%	Solution	Corrosion rate/ ($mm \cdot a^{-1}$)	Method	Corrosion type	Ref.
Mg−*x*Li− 3Al−2Zn	As-cast	5	3.5 wt.% NaCl	0.417	P_J	−	[34]
		8		8.071		−	
		14		29.591		−	
Mg−*x*Li−1Ca	As-extruded	1	Hank's solution	1.48	P_w	Integrity of the corrosion product film	[35]
		9		2.92		A mild attack	
		15		6.26		Serious corrosion	
Mg−*x*Li−1Zn	As-extruded	6	Hank's solution	0.042	P_J	Corrode partly	[36]
		9		0.158		Corrode fast	
$Mg_{94-x}Zn_2Y_4Li_x$	As-cast	0 (at.%)	Hank's solution	0.305	P_J	Galvanic corrosion	[37]
		5 (at.%)		0.165		Weaker galvanic corrosion	
		13 (at.%)		0.817		Filiform corrosion	
Mg−*x*Li	As-extruded	4	0.1 mol/L NaCl	1.848	P_w	Filiform corrosion	[38]
		7.5		3.381		A mixture of filiform and pitting corrosion	
		14		0.861		Pitting corrosion	
Mg−*x*Li− 3Al−1Zn−0.2Y	As-rolled	0	3.5 wt.% NaCl	2.637	P_J	Deep corrosion holes	[39]
		8		2.251		β-Li is corroded in priority	
		11		1.629		Uniform corrosion	
Mg−3Al−*x*Li	As-cast	4	3.5 wt.% NaCl	18956	P_J	Severe spalling of metallic particles	[40]
		8		3381.8		Less particles are removed	
		12		5300.3		Local dissolution with many pits	
Mg−*x*Li	As-rolled	4	3.5 wt.% NaCl	0.065	P_J	Partly areas corroded	[41]
		12		5.438		All areas corroded with cracks	
Mg−*x*Li	As-extruded	1	0.1 mol/L NaCl	5.67	P_w	Groove-like corrosion	[42]
		3		3.99		Prominent but slender corrosion filaments	
		5		3.15		No corrosion pits	
Mg−*x*Li− 3Al−2Zn−0.2Zr	As-extruded	5	3.5 wt.% NaCl	7.56	P_w	Intergranular corrosion	[43]
		8		4.62		β-Li phase is corroded prior to α-Mg phase	
		11		20.538		Pitting corrosion	
Mg−*x*Li− 3Al−2Zn−0.2Zr	As-homogenized	5	3.5 wt.% NaCl	12.369	P_w	Filiform corrosion	[44]
		8		6.195		Galvanic corrosion	
		11		18.438		Pitting corrosion	

P_J and P_w are corrosion rates measured by polarization and weight-loss methods, respectively

of Li soluble in Mg alloy can reduce hydrogen evolution; however, β-Li phase with high Li content significantly deteriorates the corrosion resistance of the alloy. LI et al [38] indicated that Mg−Li alloys with high Li content exhibit better corrosion resistance. It can be seen in Fig. 3 [38] that filiform corrosion occurs on the surface of α-Mg phase with low Li content in Mg−4Li and Mg−7.5Li alloys, and Mg−14Li alloy exhibits less obvious corrosion with small and slight corrosion pits. The test results of the NDE (negative difference effect) of Mg−Li alloys indicated that β-Li phase with high Li content weakens the NDE of the Mg−Li alloy due to the durable and intact surface film on it, while the rupture of the surface film caused by anode dissolution leads to the enhancement of NDE in Mg−4Li and Mg−7.5Li alloys [46]. SUN et al [44] concluded that the as-extruded LAZ832−0.2Zr exhibits the best corrosion resistance with the smallest corrosion current density of 52.30 μA/cm^2, the largest charge transfer resistance of 428.7 Ω·cm^2, and the lowest mass loss rate of 2.20 mg/(cm^2·d), while the as-extruded LAZ1132−0.2Zr alloy exhibits the worst corrosion resistance. When Mg−Li alloys with different Li contents are used as the anode of batteries, the α-Mg alloy suffers significant hydrogen gas evolution and the hydrogen evolution in β-Li alloy is memorably weakened. As shown in Fig. 4 [47], the corrosion potentials of α-Mg, $\alpha+\beta$ and β-Li alloys are −1.449, −1.526 and −1.542 V (vs SCE), respectively, and the corrosion current densities are 107.4, 97.7 and 89.1 μA/cm^2, respectively. Mg−3Al−8Li inhibits self-discharge and dissolves discharge products uniformly [40], compared with Mg−3Al alloys with 4 and 12 wt.% Li.

Based on the mentioned above, the conclusions can be drawn that the corrosion behavior of Mg−Li alloy with low Li content is similar to that of traditional Mg alloys. In the atmosphere, uniform corrosion is the dominant form, while pitting corrosion, filiform corrosion and galvanic corrosion often emerge in aqueous solution. For Mg−Li alloy with medium Li content, which often presents a dual-phase structure, the galvanic corrosion occurring preferentially at the interface is the focus of attention, as well as different corrosion types in α-Mg and β-Li phases. The effects of oxides/hydroxides/carbonates on corrosion behavior of Mg−Li alloys with high Li content are worth considering to avoid corrosion damage.

3.2 Grain size

It has been widely investigated that the grain size of alloys has a significant effect on the corrosion behavior. For Mg [48] and Mg alloys [49], there are conflicting viewpoints about the relationship between grain size and corrosion rate as well as corrosion tendency. In some cases, grain refinement can greatly enhance corrosion

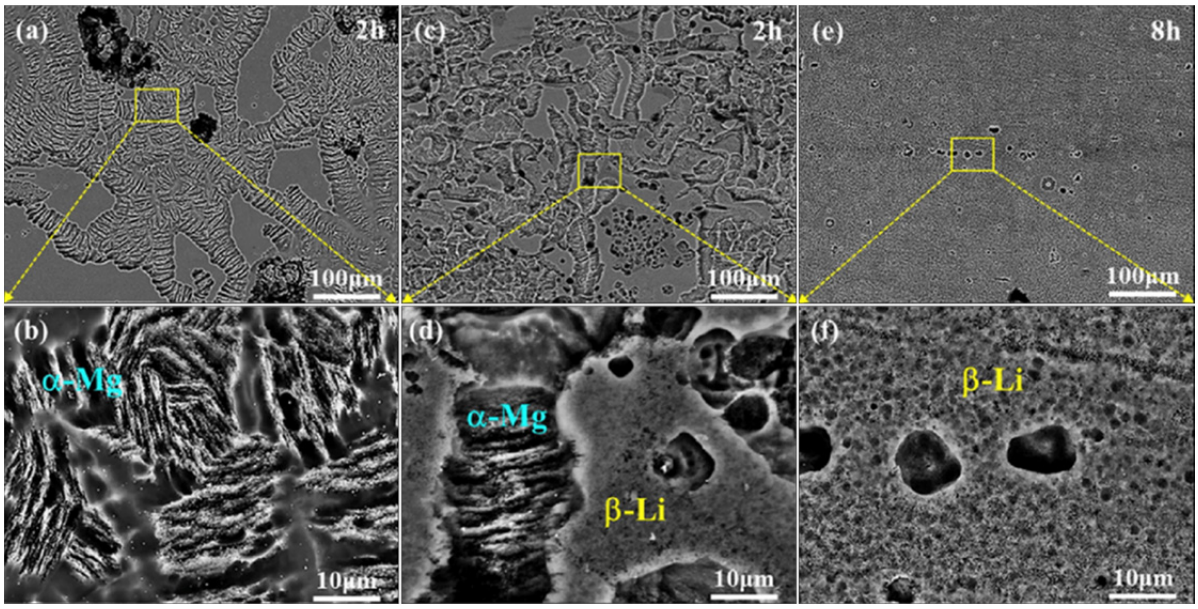

Fig. 3 SEM images of specimen surfaces following removal of corrosion products for Mg−4Li (a, b), Mg−7.5Li (c, d) and Mg−14Li (e, f) (all in wt.%) exposed to 0.1 mol/L NaCl solution for 2, 2 and 8 h, respectively [38]

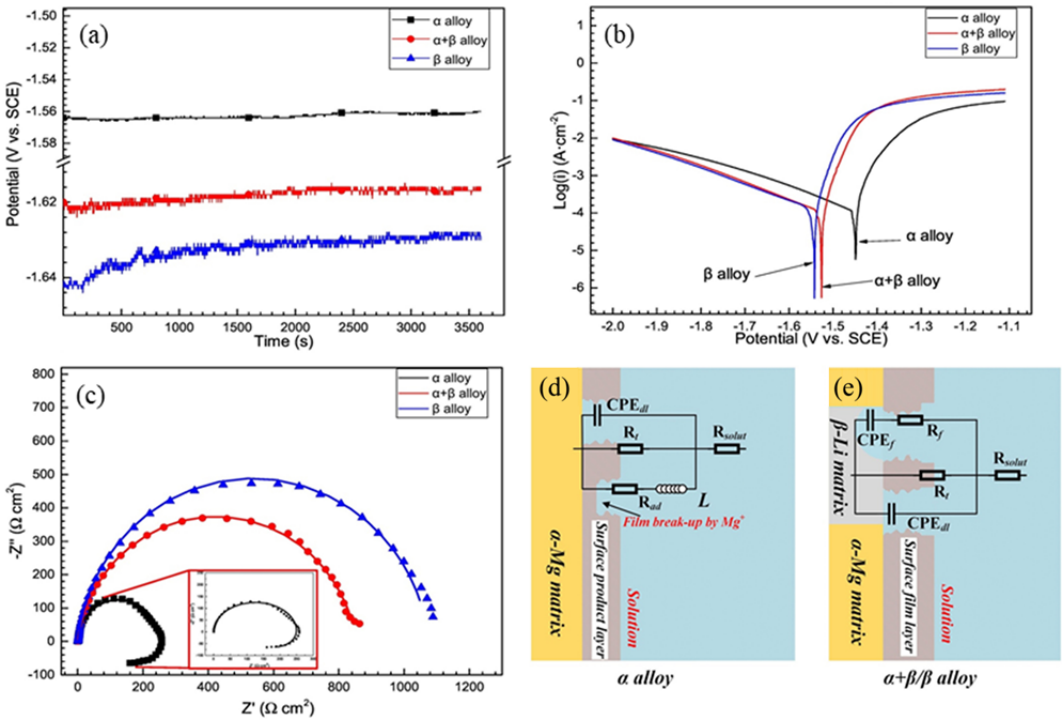

Fig. 4 Electrochemical properties of investigated alloys [47]: (a) OCP curves; (b) Polarization curves; (c) Nyquist plots; (d, e) Schematic diagrams for surface dissolving and fitted equivalent circuits of α (d), α+β and β (e) alloys

resistance, mainly because the increase of grain boundary density makes it easier to form a passive film on the surface and improves the adhesion between the oxide and the substrate. On the contrary, it is believed that smaller grains result in increasing the corrosion rate owing to the increase of defects at the grain boundaries with higher activity and faster corrosion rate. In addition, some secondary phases continuously distributed at the grain boundaries acting as barriers become isolated cathodes due to grain refinement, which will promote micro-galvanic corrosion. The grain size of Mg−Li alloys can be changed by controlling the casting process and applying various processing methods [50]. WU et al [51] prepared fine-grained Mg−13Li−X alloys by a rapid solidification process, and obtained the grain size of 4.2 μm compared to 150 μm of the traditional as-cast alloy. The alloy with fine grains has a corrosion potential (E_{corr}) of −1.354 V and a corrosion current density (i_{corr}) of 5.830×10^{-7} A/cm^2 after immersion in HBSS for 2 h. The grain refinement is beneficial to improving the corrosion resistance of the Mg−Li alloy. The introduction of ultrasonic vibration during the melt solidification process can make α-Mg phase change from coarse flower-like structure to a fine spherical structure, thus reducing the corrosion current density and corrosion products [52]. By comparing the microstructure of Mg−9Li−3Al−1Ca alloys prepared by gravity casting and centrifugal casting [53], it can be seen that α-Mg phase can be refined and spheroidized after centrifugal casting. Accordingly, the corrosion current density decreases from 220.4 to 89.4 μA/cm^2. It has been noted that the transformation from the local corrosion with large pitting pits into the uniform corrosion by means of grain refinement can effectively prevent corrosion cracks from extending to the depth of the alloy, thereby reducing the corrosion rate. As shown in Fig. 5 [54], the grains of Mg−9Li−1Zn alloy treated by friction stir are remarkably refined, with the size of α-Mg phase decreasing from 5.7 to 2.1 μm, and that of β-Li phase decreasing from 11.9 to 2.2 μm. Consequently, the corrosion current density reduces from 2.734×10^{-3} to 1.092×10^{-3} A/cm^2, with the corrosion morphology changing from local corrosion of large and deep corrosion pits to uniform corrosion of a large number of shallow and fine corrosion pits.

Table 2 lists recent literatures about the grain refinement of Mg−Li alloys through micro-alloying

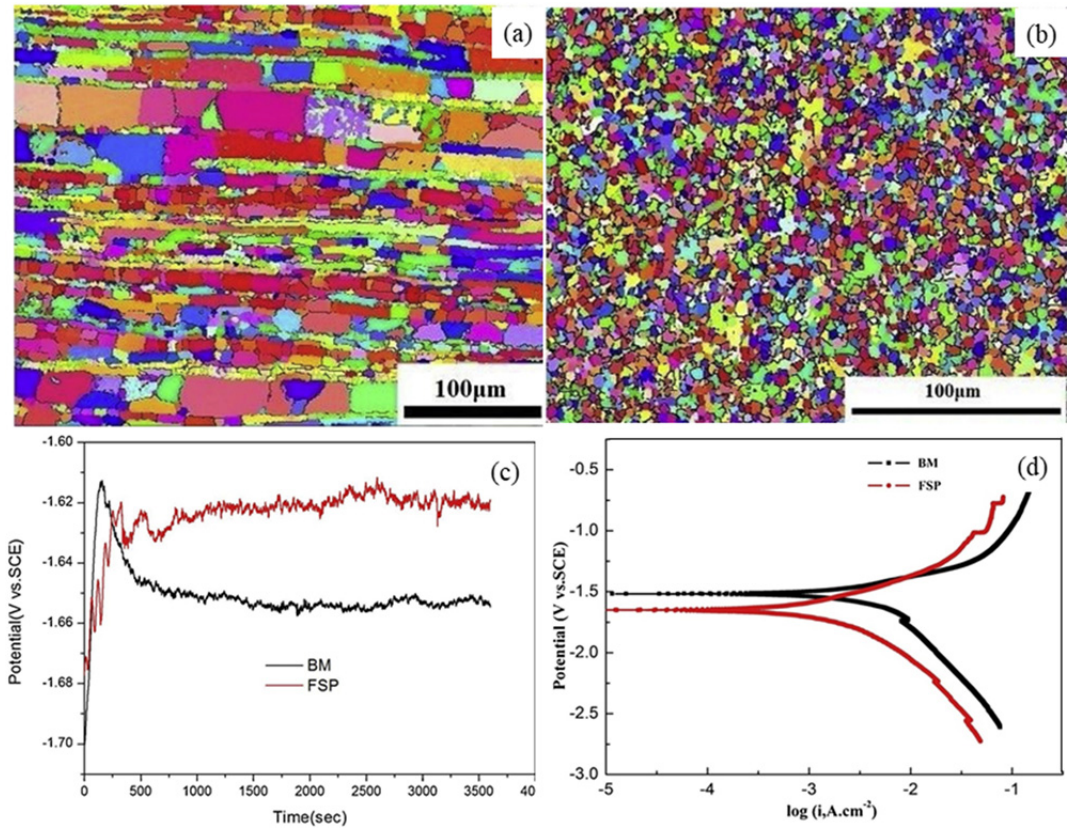

Fig. 5 EBSD maps and electrochemical properties of BM and friction stir processed alloy specimens [54]: (a) EBSD map of BM; (b) EBSD map of SZ center; (c) Open circuit potential vs time; (d) Polarization curves

Table 2 Corrosion rates of some Mg−Li alloys with different grain size

Alloy	Processing methods	Solution	Grain size/μm	Corrosion rate/(mm·a^{-1})	Ref.
Mg−4Li	Alloying-0Ca	SBF	150±10	3.89 (P_J)	[55]
Mg−4Li−0.5Ca	Alloying-0.5Ca		85±2	0.82 (P_J)	
Mg−4Li−1.0Ca	Alloying-1.0Ca		79±2	1.14 (P_J)	
LAZ832	Alloying-0Nd	3.5 wt.% NaCl	20−30	8.60 (P_H)	[56]
LAZ832−0.5Nd	Alloying-0.5Nd		α(100, 10)	3.79 (P_H)	
Mg−4Li	As-cast	SBF	150±8	244 (P_J)	[57]
Mg−4Li	Hot rolling		17±6	104 (P_J)	
Mg−4Li−1Ca	As-cast		100±5	10.7 (P_J)	
Mg−9Li−3Al−1.6Y	As-cast	0.1 mol/L NaCl	325	5.0 (P_J)	[58]
	As-extruded		75	1.65 (P_J)	
Mg−10Li−1.5Ca	As-extruded	0.6 mol/L NaCl	β(77, 28)	0.21 (P_J)	[59]
	Cold-rolled		β(59, 25)	0.11 (P_J)	
	Cryo-rolled		β(56, 21)	0.11 (P_J)	
LAE442	As-cast	In vivo	36.85	0.035 (P_J)	[60]
	Single-extruded		25.32	0.025 (P_J)	
	Double-extruded		11.27	0.0134 (P_J)	

P_J, P_w and P_H are corrosion rates measured by polarization, weight-loss and hydrogen evolution methods, respectively; SBF is short for simulated body fluid

and imposing plastic deformation, and the correlation between grain size and corrosion rate. Generally, the decrease of grain size can improve the corrosion resistance of Mg−Li alloy. However, after adding 0.5Nd to the LAZ832 alloy [56], the equiaxial α-Mg phase transformed into a long ribbon structure with 100 μm in length and 10 μm in width. Therefore, the addition of Nd leads to the grain coarsening, but it enhances the corrosion resistance of LAZ832 alloy, which is mainly affected by the second phase in the alloy. It has been reported that the corrosion rate of the alloy decreases with the increase of grain size during heat treatment, especially for solution treatment. The corrosion behavior of Mg−9Li−3Al−2.5Sr alloy at different aging temperatures (75, 100, 125, 150, 175 °C) after solution at 400 °C for 3 h was investigated by immersion test and polarization curve test, and the results showed that the corrosion resistance of the alloy aged at 150 °C is higher than that aged at 75 °C [61]. With the increase of aging temperature, the grain grows and the grain boundary area per unit volume decreases, thus improving the corrosion resistance of the alloy. GAO et al [17] observed the microstructure and corrosion behavior of Mg−3Nd−1Li−0.2Zn alloy solution-treated for different time (0, 2, 4, 8, 12 h). The grain size increases rapidly with prolonging the solution time, causing the variation of corrosion behavior. The alloy possesses the best corrosion resistance at 4 h. It can be explained that, in an active environment where the corrosion current density exceeds 10 μA/cm^2, the corrosion rate decreases with the increase of the grain size.

The uneven distribution of grain size within the alloy will also affect the corrosion performance of the alloy [62]. It is largely caused by non-uniform grain size distribution affecting uniformity of the passivation layer and the degree of segregation of impurities at the grain boundary. In the as-extruded Mg−1Li−1Ca alloy [63], the surface layer with finer grains has a better corrosion resistance than the inner layer with coarser grains. And the electrochemical differences between the inner and outer layers of grains with different sizes lead to micro-galvanic corrosion.

The following equation can be used to formulate the effect of grain size on the corrosion rate. Like the Hall−Petch type equation, the corrosion rate (CR) can be written as

$$CR=a+bD^{-0.5} \quad (11)$$

where D is the grain size, a and b are the fitting constants related to other parameters. Figure 6 shows the relationships for different Mg−Li alloys. It shows that the corrosion resistance of Mg−Li alloys can be improved by decreasing grain size in most cases.

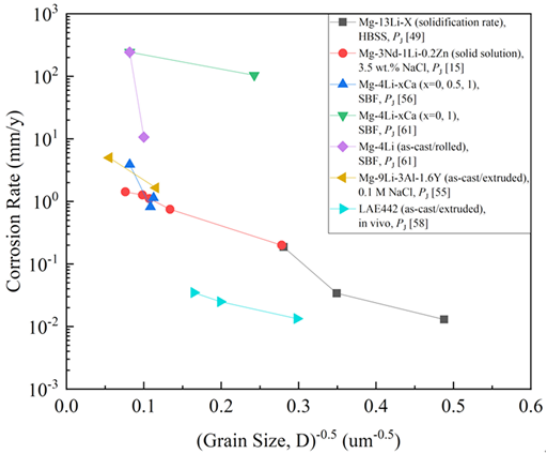

Fig. 6 Effect of grain size on corrosion rate of Mg−Li alloys (P_J, P_w and P_H are corrosion rates measured by polarization, weight-loss and hydrogen evolution methods, respectively)

Additionally, it should be noted that, the elongated grains in Mg−Li alloys obtained by deformation are detrimental to the corrosion resistance, resulting in exfoliation corrosion. There are few reports about the intergranular corrosion in Mg−Li alloys, and the effect of grain size on the corrosion resistance of Mg−Li binary alloys has been rarely reported.

3.3 Grain orientation

It is generally believed that the basal planes have better corrosion resistance in hcp Mg alloys, because the atoms on the basal plane are closely arranged and there is a high binding energy between the atoms. The dissolution rate of $(10\bar{1}0)$ and $(11\bar{2}0)$ planes is 18−20 times that of basal plane (0001) according to theoretical calculations [64]. Besides, surface energy plays a part in cathode hydrogen evolution process, through adsorbing water or protons to accelerate the hydrogen evolution reaction. The surface energies of (0001), $(10\bar{1}0)$ and $(11\bar{2}0)$ planes of Mg are 1.54×10^4, 3.04×10^4 and 2.99×10^4 J/mol, respectively [65],

indicating that the corrosion rate of (0001) plane is the lowest, followed by $(10\bar{1}0)$ and $(11\bar{2}0)$ planes. Crystal planes also affect the oxide film. (0001) orientation is beneficial to enhancing the stability of the corrosion film, thereby elevating the corrosion resistance [66]. From Fig. 7 [67,68], it can be obviously observed that the prismatic plane is vulnerable to corrosion erosion, while the basal plane has a higher corrosion potential, a lower anodic polarization current density, and a larger impedance and thinner surface film. Through hydrogen evolution, potentiodynamic polarization and electrochemical impedance spectroscopy measurements on pure Mg single crystal, it can be concluded that the corrosion rate increases in the order of (0001), $(11\bar{2}0)$ and $(10\bar{1}0)$. Figure 7(c) shows the polarization curves of different crystal planes of pure Mg [68], indicating that the anodic reaction controls the corrosion behavior related to grain orientation, and the charge transfer and film resistance are strongly orientation dependent.

The influence of different crystal plane orientations on corrosion behavior of Mg−Li alloys is mainly focused on the single-phase α-Mg with hcp structure, and the conclusions obtained are similar to those of traditional Mg alloys. ZHANG et al [69] found that the surface grain orientation in hcp Mg−4Li alloy with a strong matrix texture mainly corresponds to $(10\bar{1}0)$ and $(11\bar{2}0)$ after the addition of Al−Si eutectic alloy, and the corrosion resistance of the alloy decreases. The same results were observed when Al was added to Mg−4Li [70]. YANG et al [71] studied the corrosion behaviors of LAZ131 and LAZ531 at open circuit potential and concluded that $(10\bar{1}0)$ and $(11\bar{2}0)$ oriented grains are more susceptible to corrosion than (0001) oriented grains. Due to the different deformability of α-Mg phase and β-Li phase, different types of textures of α-Mg phase and β-Li phase have different impacts on corrosion properties of Mg−Li alloys.

By comparing the corrosion properties of as-rolled Mg−8Li alloy plates with different orientations, it has been demonstrated that there is obvious corrosion anisotropy between the surfaces of different oriented plates, as shown in

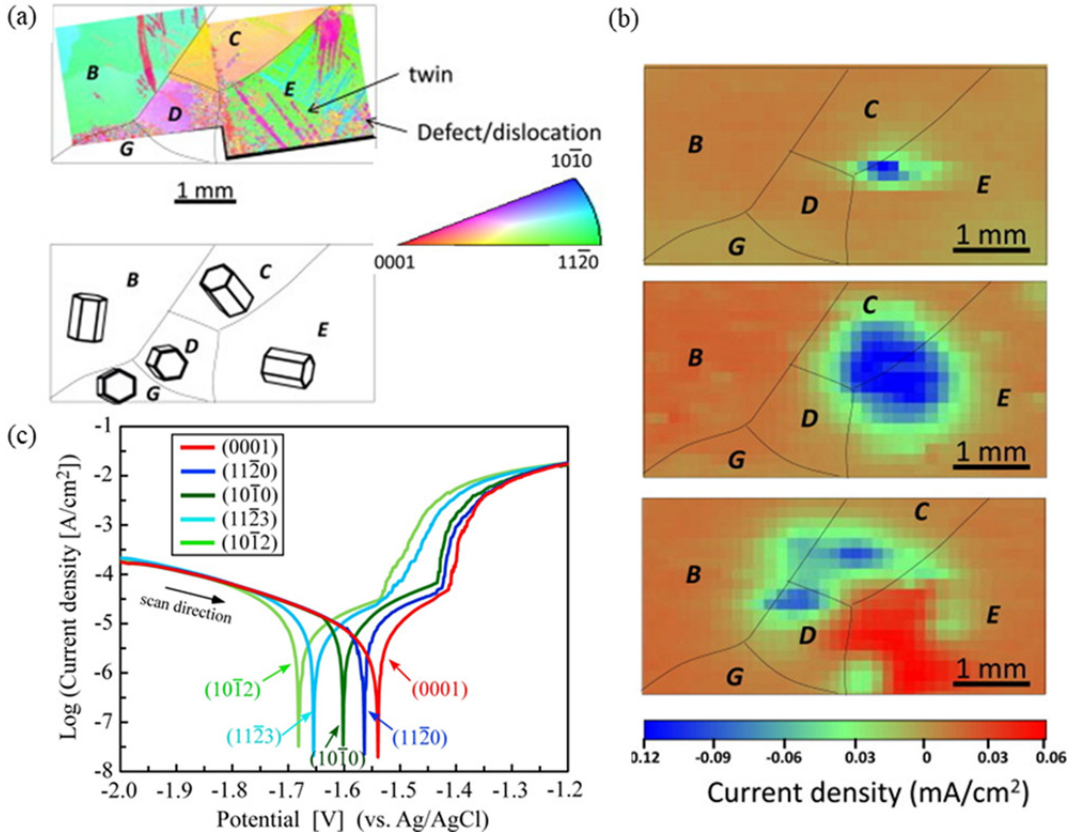

Fig. 7 (a) EBSD grain distribution and schematic illustration of grain orientations of Mg coupon [67]; (b) SVP maps of Mg coupon obtained at 0, 60 and 180 min after immersion in 0.01 mol/L NaCl [67]; (c) Potentiodynamic polarization curves of pure-Mg−SCs in HBSS at 37 °C, with exposed surface parallel to (0001), $(10\bar{1}0)$, $(11\bar{2}0)$, $(11\bar{2}3)$, and $(10\bar{1}2)$ [68]

Fig. 8 [72]. The corrosion rate of "ND" samples with the surface perpendicular to the normal direction of the plate is the highest, that of "TD" samples with the surface perpendicular to the transverse direction is the second, and that of "RD" samples with surface perpendicular to the rolling direction has the lowest corrosion rate. The variation of corrosion behavior is mainly ascribed to crystal structure of the α-Mg phase. For the "ND" and "TD" plates, the exposed surfaces are composed of (0002), $(10\bar{1}0)$ and $(11\bar{2}0)$ planes, leading to severe corrosion between the base surface and the prism surface. However, the "RD" sample did not suffer micro-galvanic corrosion due to the $(10\bar{1}0)$ and $(11\bar{2}0)$ crystal planes on the surface. In order to optimize the grain orientation and tailor the anisotropy of the alloy, the addition of rare earth elements, pre-deformation and annealing are commonly put into effect. The texture of Mg−4Li alloy can be weakened by adding Zn and Y elements to form I phase (Mg_3Zn_6Y, icosahedral structure) [73]. HE et al [74] suggested that the re-orientation of the prismatic planes through pre-deformation effectively enhances the corrosion resistance of the sheet. The texture of as-extruded LAZ331 sheet gives rise to poor corrosion resistance due to a large number of high surface energy prismatic surfaces parallel to the surface, and pre-deformation reduces the number fraction of high-surface energy prismatic planes from 91% to 6%, as well as corrosion current density from 126.1 to 32.0 μA/cm^2.

The corrosion performance of Mg alloys depends not only on the concentration of basal planes, but also on the twins formed in the alloy. ZOU et al [75] reported that $(10\bar{1}2)$ tensile twinning improves corrosion properties by changing the pitting potential, film formation sequence and charge transfer resistance. On the one hand, twinning causes the turning of crystal orientation, contributing to the ratio of the basal plane to the prism plane. On the other hand, the twinning zone and the twinning boundary are more active, leading to a potential difference with the matrix.

The LA51 and LAZ531 alloys exhibit extension twinning and the twinning density increases with the increase of rolling reduction [76]. There is an obvious passivation tendency on the anode side of the polarization curve of LA51 alloy plates with rolling reductions of 15% and 20% [65]. It is mainly determined by the $(11\bar{2}0)$ extension twinning accelerating the formation of the oxide film. By contrast, the twinning in LAZ531 alloy increases the corrosion rate [77].

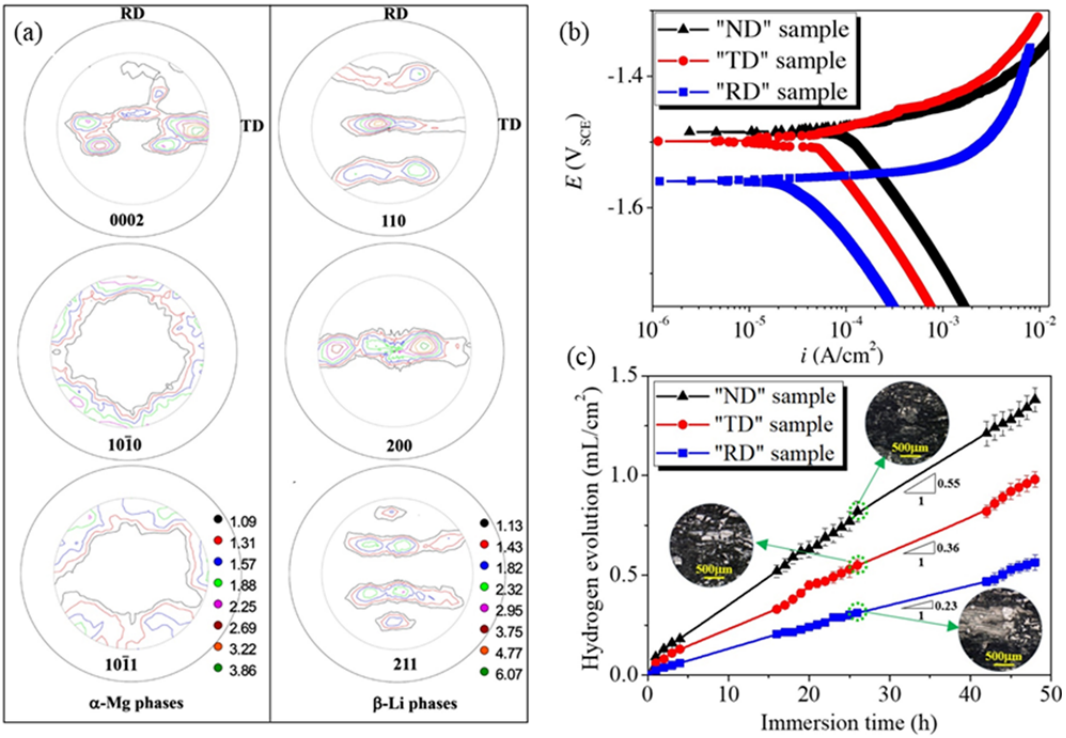

Fig. 8 Macro texture analysis of as-rolled Mg−8wt.%Li alloy (a), potentiodynamic polarization curves (b) and hydrogen evolution curves of "ND", "TD" and "RD" samples measured in 0.1 mol/L NaCl solution (c) [72]

The effect of grain orientation on the corrosion behavior of Mg−Li alloys is mainly concentrated in the hcp structure with low Li content. In order to improve the corrosion resistance of Mg−Li alloys, the grain orientation can be optimized so that the (0001) base plane is parallel to the surface. As β-Li phase reduces the anisotropy of Mg−Li alloys, the variability of corrosion in different surfaces of Mg−Li alloy after deformation is attributed to the amount and distribution of α-Mg phases. However, there are few works about the corrosion anisotropy of pure β-phase presently.

3.4 Second phase

It is well known that the second phase has a remarkable influence on the corrosion properties of Mg alloys. One of the reasons is the galvanic corrosion between the second phase and the matrix. The potential values of various second phases in Mg alloy are summarized in Table 3 [78,79]. It can be seen that most of the second phases are cathode relative to the matrix, and Al−Fe and Al−Mn are the most harmful cathode phases, strongly promoting the corrosion of the Mg matrix. The $Mg_{17}Al_{12}$ phase located along the grain boundary in the AZ alloys acts as a cathode for accelerating the hydrogen evolution reaction or as a corrosion barrier for hindering the damage, mainly depending on the volume fraction and distribution of the $Mg_{17}Al_{12}$ phase. The additions of La, Nd, and Y, etc will form the anode second phases for preferentially degradation [80−82]. In Mg−Li alloys, Li-containing phases are also produced in addition to the common second phases in traditional Mg alloys above mentioned.

Due to the electrochemical difference between α-Mg phase and β-Li phase in dual-phase Mg−Li alloys, galvanic corrosion easily occurs. Figure 9 displays the local potential around the α-Mg/β-Li interface and grain boundary inner β-Li phase [31]. The potential difference promotes micro-galvanic corrosion. In addition, the morphology and the distribution of α-Mg phase also play great role in the corrosion performance of Mg−Li alloy [83]. The

Table 3 Potentials of intermetallics with matrix for Mg alloys [78,79]

Alloy	Phase	Potential to E_{Mg}/mV	Alloy	Phase	Potential to E_{Mg}/mV
Mg	−	0	Mg−Si	Mg_2Si	210
Mg−8Li	AlLi	380	Mg−Al	Al−Mn	370
Mg−8Li	β-Li	175	Mg−Al	Al−Fe	1050
Mg−Al	$Mg_{17}Al_{12}$	300	Mg−Al−Gd	Al_2Ca	90
Mg−Zn	$MgZn_2$	510	Mg−Al−Nd	Al_2Nd	140
Mg−Y	$Mg_{24}Y_5$	50	Mg−Al−Y	Al_2Y	320
Mg−Ce	$Mg_{12}Ce$	150	EW75	Mg−Nd−Y	−35
Mg−Ca	Mg_2Ca	−100	ZE41	Mg−Zn−RE	100
Mg−Nd	Mg_3Nd	100	TZXM4411	Mg−Sn−Zn	200

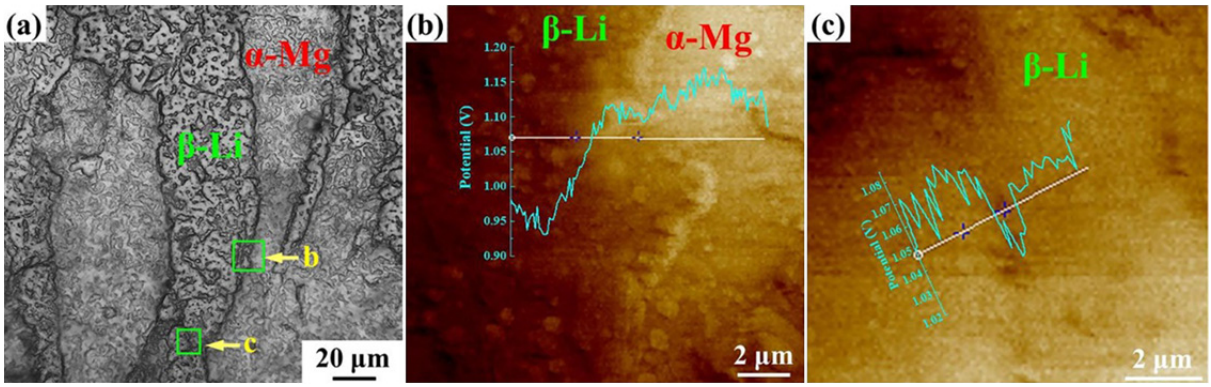

Fig. 9 SEM image (a) and local potential distribution at α-Mg/β-Li interface (b) and grain boundaries of β-Li phase (c) in eutectic Mg−8Li alloy [31]

AlLi phase can be more commonly observed in Al-containing Mg−Li alloys attributing to higher electronegativity difference of Al and Li (0.63) than that of Mg and Al (0.3) [84]. The potential of AlLi phase (−1.960 V (vs SCE)) is more negative than that of Mg matrix (−1.258 V (vs SCE)), which prefers to dissolve due to galvanic corrosion [85]. Corrosion spreads along AlLi phase forming filiform corrosion, which is mainly distributed at grain boundary and inside *β*-Li phase, and the corrosion rate increases with the increase of volume fraction of AlLi phase in Mg−Li alloy. The addition of rare earth elements such as Y [86] or Nd [87] inhibits the formation of AlLi phase and improves the corrosion resistance.

The quasicrystal phase and LPSO in Mg−Li alloy also play an important role in corrosion properties. XU and HAN [88] found that Mg−6Li−6Zn−1.2Y alloy contains *I* phase at grain boundaries, which effectively inhibits the growth of corrosion pits and the extension of filiform corrosion, thus slowing down the corrosion of dual-phase Mg−Li alloy. The microstructure and corrosion behavior of the as-extruded Mg−6.5Li−*x*Y−*y*Zn alloy were revealed by LI et al [89]. In terms of microstructure, the Mg−6.5Li−0.8Y alloy contains *α*-Mg, *β*-Li and Mg_2Y phases, Mg−6.5Li−0.8Y−0.3Zn alloy is composed of *α*-Mg, *β*-Li and *X* ($Mg_{12}ZnY$, LPSO) phases, and Mg−6.5Li−1.0Y−1.0Zn alloy is composed of *α*-Mg, *β*-Li and *W* ($Mg_3Zn_3Y_2$) phases. From the surface morphology and depth of corrosion pits, Mg−6.5Li−0.8Y−0.3Zn alloy with the lowest volume of second phase presents the best corrosion resistance, as a result of reducing the micro-galvanic corrosion. The LPSO phase acts as a barrier between the matrix and the eutectic phase to weaken the galvanic corrosion [37].

The reason that the second phase affects the corrosion resistance mainly includes the potential difference between the second phase and substrate, the amount and distribution of the second phase, and the role of the second phase opposing surface film. Some potential values of intermetallics are listed in Table 3. HU et al [90] observed Al_2Gd/Mg_2Sn/AlCuMg particles formed in the as-extruded LA83−1.2M (M=Gd, Sn, Cu) alloy, and the potential differences between these particles and the matrix determine the corrosion rate of the alloy. The potential difference of constituents relative to the *α*-Mg phase in the alloys follows the order of AlCuMg (~680 mV) > AlLi (~340 mV) > Al_2Gd (~250 mV) > *β*-Li (~135 mV) > Mg_2Sn (~60 mV). The as-extruded LA83−1.2Cu alloy with more noble AlCuMg particles presents the maximum mass loss rate of (99.8±0.8) mg/(cm^2·d) and the maximum hydrogen evolution rate of (70.4±0.7) mL/(cm^2·d), and the micro-galvanic couples of Al_2Gd/*α*-Mg with smaller potential differences decrease the mass loss by ~70%. Therefore, it is a good strategy to reduce the potential of the cathode phase such as Al−Fe/Al−Mn by adding alloying elements to slow down the galvanic corrosion [91]. It is proved that the amount and size of $Mg_{41}Nd_5$ second phase in Mg−3Nd−1Li−0.2Zn alloy decrease with the increase of solution treatment time. After solution treatment at 535 °C for 6 h, the uniform distribution of $Mg_{41}Nd_5$ second phase results in smaller and shallower pitting pits [17]. The cross-cold rolled Mg−Li−Ca alloy possesses smaller second phases evenly dispersed in the matrix than cold rolled alloy, which promotes the formation of uniform and dense corrosion products on the surface according to the corrosion morphology [59]. It is also observed that the protective surface film forms in the as-extruded Mg−1.21Li−1.12Ca−1Y alloy due to the fine and uniformly distributed second phase [92].

As for the second phases in Mg−Li alloys, special attention should be paid to the purification of the alloy as for reducing the harmful impurities in the alloy and avoiding forming strong cathode phase. The volume fraction of AlLi phase in the Mg−Li−Al alloy ought to be reduced by adding alloying elements since the AlLi phase is detrimental to the corrosion resistance of Mg−Li alloy. Similar to $Mg_{17}Al_{12}$ phase at grain boundaries, it is encouraged to form network phase with barrier effect for the sake of slowing down the corrosion. In addition, small and uniform distributed second phase can enhance corrosion resistance of Mg−Li alloys.

3.5 Surface film

The composition and structure of the corrosion film formed on the surface of Mg and Mg alloys affect the corrosion rate of the alloy. It is expected to form a dense and stable oxide film to effectively prevent air or ions from further contacting the metal substrate. Mg can spontaneously form a thin but

dense oxide film in the air, mainly composed of MgO and $Mg(OH)_2$ with an amorphous structure [93]. In the humid air, the outer layer usually forms a 20−40 nm surface film, and the inner layer belongs to a multicellular amorphous hydration layer [94]. However, the surface film of Mg alloy naturally formed in aqueous solution is generally loose and porous without effective protection for Mg alloy [94].

Affected by the active Li element and different crystal structures, the composition and structure of Mg−Li alloy surface film exhibit particular characteristics. LI et al [95] investigated the characteristics and the protective properties of the surface film of pure Mg with hcp structure and Mg−14Li alloy with bcc structure, indicating that typical flaky $Mg(OH)_2$ particles form on pure Mg. The articulated need-like particles are observed on the surface of Mg−14Li, with a thickness of up to 4 μm and some tiny holes within it, as shown in Fig. 10 [95]. It has been shown that both surface films may decompose under high anode overvoltage. In Mg−Li−Al alloys, higher Li content results in a thicker oxide film. In addition, the dual-phase Mg−Li alloys are propitious to a thicker oxide film due to accelerated corrosion of the primary battery [96]. Because of Li addition, not only the surface film composition of Mg−Li alloys includes Li-containing compounds, but also the surface film has a typical multilayer structure. Four

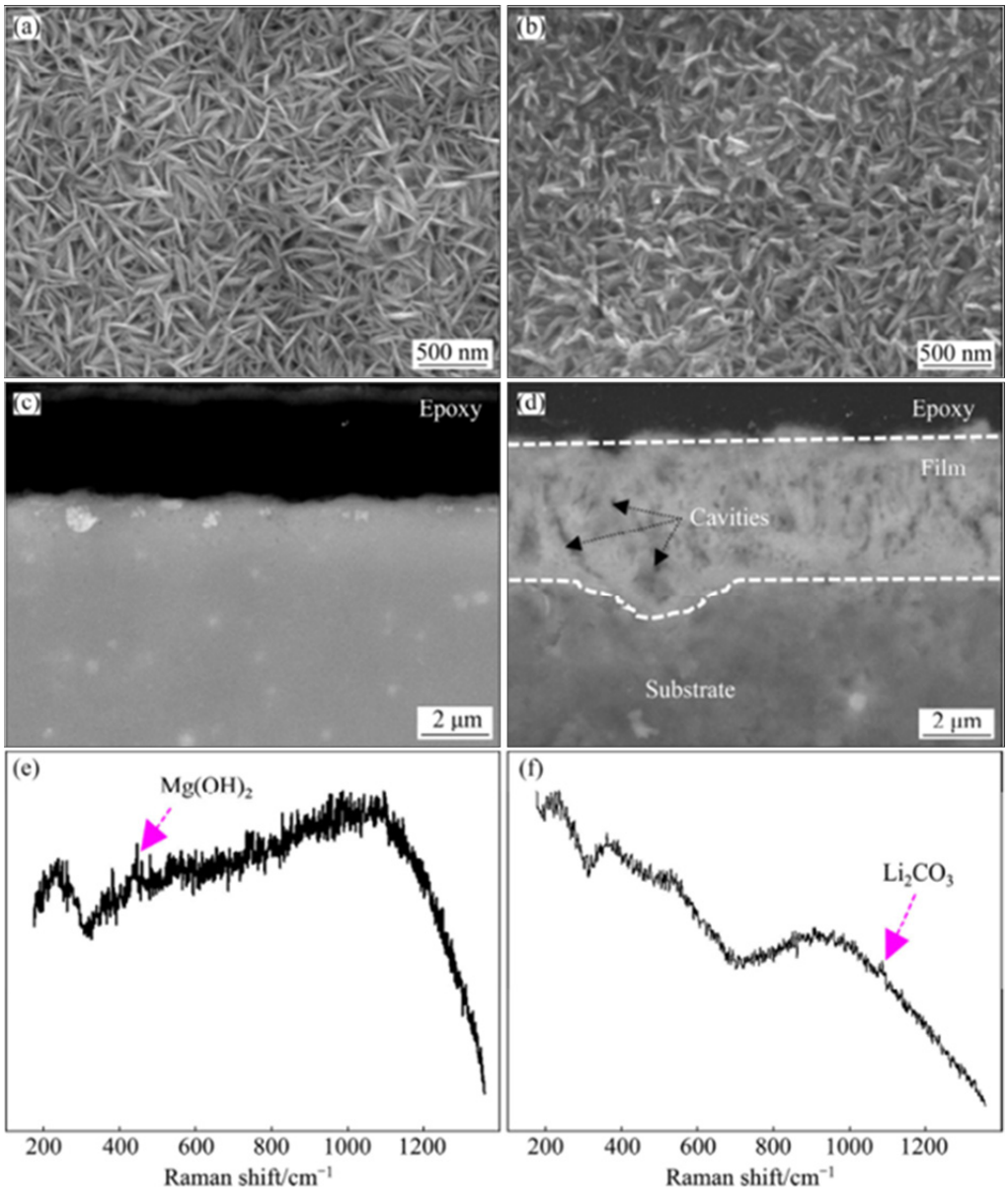

Fig. 10 Planar (a, b) and cross-sectional (c, d) morphologies and Raman analysis (e, f) of surface film on pure Mg (a, c, e) and Mg−14Li alloy (b, d, f) exposed to 0.1 mol/L NaCl for 8 h [95]

layers formed on the surface of Mg−8Li alloy in the ambient atmosphere include: the top layer being the mixture of $Mg(OH)_2$ and Li_2O; the second layer being the mixture of $Mg(OH)_2$, Li_2O and MgO; the third layer being the mixture of $Mg(OH)_2$, MgO, LiOH, Li_2O and Mg; the bottom layer being the mixture of MgO, Li_2O, Li and Mg [97]. The Mg and Li in Mg−Li base alloys are easily oxidized to form MgO and Li_2O, and they will be partially converted to hydroxides when contacting H_2O molecules. The thermodynamic function H_0 determines that $Mg(OH)_2$ and Li_2O exist stably in the surface film. ZENG et al [98] disclosed that the oxide film of Mg−Li alloy exposed to the air for a long time also presents a four-layer structure, and the outer layer is composed of Li compounds (Li_2O, LiOH and Li_2CO_3). The principle of the reaction is that Li ions easily diffuse from the interface of metal and oxide to the outer layer of oxide on the base of the small diameter, fast diffusion speed and high reaction activity of Li atom. Time of flight-secondary ion mass spectrometry (ToF-SIMS) was used to investigate the surface as well as bulk microstructural features of novel Mg−Li−Al based alloy by KUMAR [99], indicating that there are six multi-oxide layers within the surface film of LATZ9531. The surface film mainly contains Li, Mg and Al, and the Li content gradually decreases from the sample surface to the inside of the matrix.

Some alloying elements are beneficial to the formation of thinner, denser, more stable and more protective oxide film [100]. With the addition of Y to LAZ832 alloy, lots of tiny erect flakes perpendicular to the surface make the oxide film denser and more protective and prevent further corrosion of the matrix [86]. The addition of YAl_2 in Mg−Li alloy stimulates the formation of Y_2O_3 on the surface, which enhances the binding force between the oxide film and the substrate [101]. The dense film containing Y_2O_3, Al_2O_3 and Li_2CO_3 can hinder further development of pitting corrosion. Similarly, the addition of Nd can also form Nd_2O_3 on the surface of the alloy, change the structure of the corrosion film, inhibit the penetration of harmful ions, and improve the corrosion resistance [55]. The protective effect of the oxide film on the metal substrate is usually measured by Pilling−Bedworth ratio (PBR) [102]. PBR is the ratio of the oxide volume to consumed metal volume, which reflects the stress state, integrity or compactness of oxide film. It is generally believed that, when PBR>1, compressive stress exists in the oxide film, while tensile stress is generated in the oxide film at PBR<1. The greater the difference between PBR value and 1 is, the greater the stress is, and the easier it is to cause rupture of surface oxide film. The common compounds in Mg−Li alloy surface film and their PBR values are listed in Table 4 [22]. It can be known that, among the compounds containing Li, Li_2CO_3 and LiOH are the protective oxide film components.

Table 4 PBRs of some chemical compounds [22]

Compound	PBR
Li_2O	0.57
MgO	0.80
LiOH	1.26
$Mg(OH)_2$	1.80
Li_2CO_3	1.35
$MgCO_3$	2.04

XU et al [32] and HOU et al [103] believed that the high corrosion resistance of Mg−10.95Li−3.29Al−0.19Zr−0.59Y alloy lies in the formation of a protective uniform Li_2CO_3 oxide film on the surface of the alloy. YAN et al [104,105] systematically investigated the compositions of surface films on Mg−Li(−Al−Y−Zr) alloy formed in the air and the aqueous solution. The surface cross-section prepared by focusing ion beam (FIB) was observed and analyzed, and the structure of the oxide film was characterized by glow discharge optical emission spectroscopy (GD-OES). A complex and multi-layer surface film forms upon Mg−Li(−Al−Y−Zr) alloy, mainly containing Li_2CO_3 and $Mg(OH)_2$. Li is distributed in the entire surface film, and the concentration is higher in the outer layer with a relatively porous layer. The Li-containing compounds in the inner layer are mixed with products to form a relatively dense layer, which improves the corrosion resistance, as shown in Fig. 11 [104]. By means of in-situ surface analysis of the alloy immersed in aqueous solution, it can be found the Li-doped MgO film with about 100 nm is formed to inhibit the transformation of MgO into $Mg(OH)_2$, which increases the chemical stability of the surface film by completing the charge compensation of the polar surfaces and point

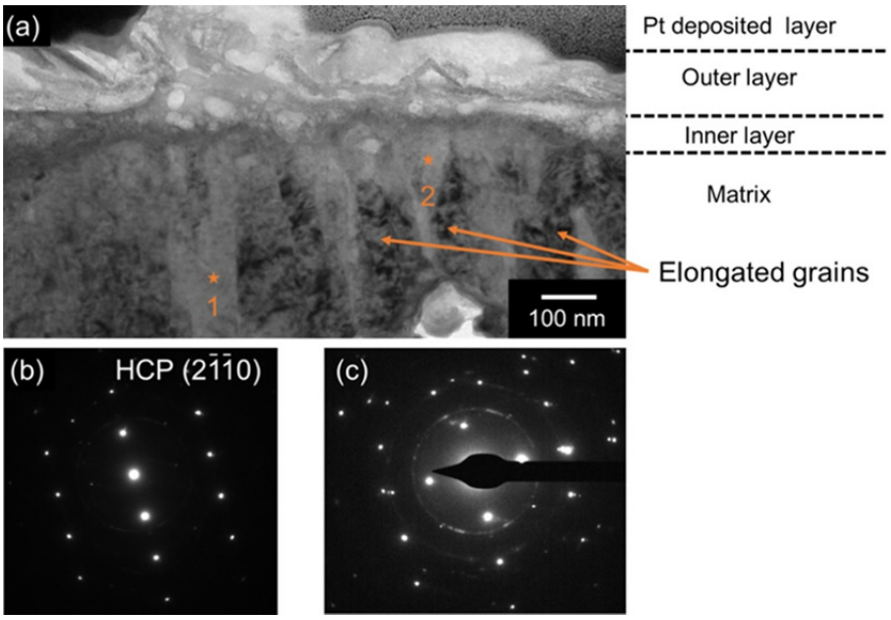

Fig. 11 Bright field TEM image of cross-sectional surface lamella from Mg−Li(−Al−Y−Zr) alloy following 24 h of immersion in 0.1 mol/L NaCl and exposure to air for 7 d (a), and SAED patterns collected from positions marked as "1" (b) and "2" (c) in (a), respectively [104]

defects. Additionally, the generated Li−Al-LDH ($Li_2[Al_2(OH)_6]_2{\cdot}CO_3{\cdot}nH_2O$) also inhibited cathodic activation and reduced corrosion rate [33].

It has been recognized that Li_2CO_3 in the surface film plays a role in corrosion resistance. It is readily formed under the exposure to CO_2 in the air. In aqueous solutions, the main products are oxides and hydroxides of Mg and Li, so that the role of the existence and diffusion of Li on the stability of these products deserves more investigations. In addition, the influence mechanism of rare earth elements on oxides and corrosion resistance of Mg−Li alloys needs to be further researched in detail. Presently, advanced detection and analysis techniques make it possible to investigate the reaction processes in situ and at a much smaller scale.

3.6 Other factors

Dislocation and stress in the corrosion of Mg alloys have been identified as potentially important factors [106]. Dislocation means the crystallographic defects and distortions. The atoms at dislocations are more susceptible to corrosion. Therefore, a higher dislocation density increases the anodic dissolution of Mg alloys and reduces the equilibrium potential near the dislocations, leading to the passive film unstable and easy to be destroyed. Dislocation plugging at the grain boundary causes the grain boundary to be easily damaged at initial corrosion. VAUGHAN et al [107] found that the corrosion of ECAP-processed Mg alloy accelerates due to uneven anodic shear zones, where a large number of fine grains and precipitates concentrate. For residual stress, the residual tensile stress is unfavorable to the corrosion resistance of Mg alloy, while the residual compressive stress can improve the corrosion resistance. This is because the residual compressive stress offsets part of the transverse tensile stress caused by the accumulation of corrosion products, thus slowing down the cracking and damage of the oxide film.

The corrosion behavior of Mg alloys is closely related to the corrosive environment, and it presents an apparent difference in gas and solution. In aqueous solution, the corrosion rate of Mg−Li alloy is significantly changed by pH value, solution composition, temperature and flow rate [108]. The corrosion resistance of Mg−8Li alloy in the air can be significantly improved by increasing Al content, while it decreases with the increase of Al content in NaCl solution [109]. The corrosion rate of Mg−11Li−3Al−0.5RE alloy in NaCl solutions with different concentrations (0.01, 0.05, 0.1 and 0.5 mol/L) at pH 9 is 203.7, 270.0, 412.6 and 1283.6 mg/($m^2{\cdot}$h), respectively, while that at pH 12

is lower. With the increase of pH value, E_{corr} moves to the positive direction and there exists obviously passivating stage in the process of corrosion at pH 12, which indicates that the corrosion rate is slowed down [110]. WITTE et al [111] also reported that there was a significant difference in the corrosion rate of LAE442 alloy in vivo and in vitro, which is about 4 orders of magnitude lower in vivo than that in vitro. Moreover, the corrosion rate of Mg−4Li alloy in 0.1 mol/L NaCl, 3.5 wt.% NaCl solution and SBF is 1.848 mm/a (P_w) [38], 0.065 mm/a (P_J) [41] and 244 mm/a (P_J) [57], respectively.

4 Processing methods for corrosion behavior of Mg−Li alloys

4.1 Alloying

Alloying is a common method to change the corrosion properties of Mg−Li alloys. On the one hand, alloying elements affect the composition and structure of surface oxide film during corrosion, for the reason that the oxide/hydroxide formed on the surface of Mg cannot provide passivation effect like Al and Cr oxides. By adding Al, rare earth and other alloying elements, the oxides, such as Al_2O_3, Y_2O_3 and Nd_2O_3, are expected to make the surface film compact and uniform, and play a stable, sustainable and repairable protective role. On the other hand, the addition of alloying elements changes the microstructure of the alloy, which mainly affects the corrosion kinetics of the Mg alloy. The solid solubility of alloying elements in Mg determines to form Mg-based solid solutions, intermetallic compound phases or impurity particles, which have an important impact on the corrosion performance of Mg alloys [48].

4.1.1 Impurity element of Fe

The influence of impurity elements on the corrosion resistance of Mg−Li alloys quite differs from that in conventional Mg alloys. For Mg alloys, minute iron element deteriorates the corrosion resistance of Mg alloy and there is a threshold concentration, that is, the corrosion rate increases rapidly when the content of iron element exceeds 0.016%. However, in LA141 alloy [112], the corrosion rate increases linearly with increasing Fe content without threshold. The absolute value of corrosion rate of LA141 alloy with trace amounts of Fe is not remarkably higher compared to commercial hcp-structured Mg alloys.

4.1.2 Common elements

Al, Zn and Ca are common alloying elements added in Mg−Li alloys. Al dissolved in Mg−Li alloys will increase the hydrogen overvoltage of the alloy and improve the structure and composition of the oxide film. The degradation rate of LAZ631 alloy with high Al content is slower than that of LAZ611 alloy in vivo, mainly because the increase of Al content forms a more stable layer, which is conducive to passivation of the surface [113]. When adding a bit of Al, it is observed that the dendrite crystals transform to equiaxial crystals and the grain size is obviously reduced [114]. With the increase of Al content, more $Mg_{17}Al_{12}$ and AlLi phases form micro-galvanic couples with the matrix to accelerate corrosion. When different contents of Al are added to Mg−14Li alloy, the volume fraction of AlLi phase increases with the formation of a network at the grain boundary, and the corrosion rate decreases firstly and then increases [84]. LV et al [115] revealed that Mg−8Li−3Al−1Zn electrode has a more positive corrosion potential and a smaller corrosion current density than Mg−8Li−3Al−0.5Zn electrode in 0.7 mol/L NaCl solution, due to fine and uniform products on the surface. The addition of Ca to Mg−4Li [55], Mg−7Li−3Al [116] and Mg−14Li [117] reduces the grain size and improves the corrosion resistance. However, as the content of Ca increases, the $(Mg,Al)_2Ca$ phase will accelerate the galvanic corrosion.

4.1.3 Rare elements

The addition of rare elements (RE) to Mg−Li alloys can bring about many advantages, such as purification of melt, grain refinement, reduction of the potential difference between the second phase and the matrix, and modification of the composition and structure of the surface film. Y has the same standard electrode potential (−2.372 V (vs SCE)) as Mg, and a dense layer of Y_2O_3 can be generated on the alloy surface, causing the improvement of corrosion resistance [118]. The addition of Y to Mg−8Li−3Al−2Zn alloy promotes to form Al_2Y phase at the grain boundaries, changing the shape of α-Mg from long needles to round ones, and reducing the amount of AlLi phase. Since the potential difference between Al_2Y phase and β-Li phase is greater than that between α-Mg phase and β-Li phase, the galvanic corrosion between β-Li phase and α-Mg phase is inhibited, and the

corrosion inside β-Li phase is weakened by the reduction of AlLi phase amount. The corrosion current densities of LAZ832 and LAZ832-1.5Y alloys are 83.757×10^{-6} and 21.065×10^{-6} A/cm^2, respectively, indicating that the corrosion rate is significantly reduced due to the addition of Y [86]. The diffusion of Al and Y atoms in the Al_2Y/LA143 composite promotes the formation of Al_2O_3 and Y_2O_3, prevents the diffusion of Cl^- ions to the matrix, and reduces the long-term corrosion rate of the alloy [101]. Sn and Y reduce the grain size and the formation of AlLi phase in Mg−5Li−3Al−2Zn alloy, resulting in shallower corrosion pits and cracks, as well as smaller corrosion current of 9.304×10^{-5} A/cm^2 [85].

Similarly, Ce [119], Nd [56] and Gd [90] are conducive to the formation of the second phase of Al_2(Ce,Nd,Gd) in Mg−Li−Al alloys, which also play role in refining the grains, inhibiting the precipitation of AlLi and $MgLi_2Al$ compounds, and weakening the micro-galvanic corrosion between β-Li phase and Al-rich particles. Rare earth elements also affect the corrosion performance and discharge performance of Mg−Li alloys as battery anode materials. The addition of Y [120,121] and La [122] can improve the electrochemical activity and corrosion resistance of the alloy, thus improving the performance of the battery.

4.1.4 Other elements

Mn can purify Fe impurities and effectively refine the grains and the second phase. The addition of Mn to the $Mg_{89-x}Y_4Zn_2Li_5Mn_x$ alloy makes the corrosion potential more positive, with the current density of the cathode branch significantly reducing and the anode branch having a tendency of pseudo passivation [123]. The corrosion rate of Mg−Li−Sn alloy is related to the content of Sn in the matrix and the amount of Mg_2Sn phase [85]. The dissolved Sn participates to form the oxide film, while Mg_2Sn promotes pitting and filiform corrosion with accelerating the corrosion rate. Zr, with a low solid solubility (0.73 at.%) in Mg alloys, does not form intermetallic phases with Mg [124]. So, the addition of Zr usually aims to refine the grains. Excessive Zr increases the Zr-containing particles at the grain boundary, resulting in micro-galvanic corrosion with the surrounding Mg matrix and damaging the surface protective oxide film. The so-called cathodic poisons, such as As, Ge, and Sn, slow down the hydrogen evolution reaction by inhibiting the formation of H_2 at the cathode. A small amount of Ge in Mg−11Li−xGe (x=0, 0.3, 0.5 wt.%) alloy improves the corrosion resistance of the alloy by reducing the cathode dynamics and promoting the formation of pseudo-passivation film on the surface [125].

Generally, the corrosion rate of Mg alloys is higher than that of pure Mg with the value of 0.3 mm/a. When lithium is added, the corrosion rate of Mg−Li alloy is much higher than that of pure Mg. Here, it is indicated that how other alloying elements affect the microstructure and corrosion behavior of Mg−Li alloys as the substrate. Aiming at improving the corrosion resistance of Mg−Li alloys, it is suggested that alloying elements should be in favor of forming a second phase with a small potential difference and accelerating a protective film. It is shown that, when multiple alloying elements are added to Mg−Li alloy at the same time, there are differences among the influence on corrosion behavior. As reported, the sequence of alloying elements affecting the corrosion resistance of the Mg−Li−Al−(Y) alloys is Al>Li>Y [126].

4.2 Deformation

Extrusion, rolling, severe plastic deformation and other mechanical deformations can change the microstructure of the Mg−Li alloy, and then affect the corrosion behaviors. Mechanical deformation causes modifications in the microstructure such as grains, second phases, dislocations and twins, which have inconsistent effects on the corrosion rates of different Mg alloys. CAO et al [127] reported the corrosion properties of hot-rolled Mg−X alloys (X=Gd, Ca, Al, Mn, Sn, Sr, Nd, La, Ce, Zr or Si) and suggested that the corrosion rate of most Mg−X alloys decreases after hot rolling due to the obvious refinement and uniform distribution of the second phase, but the iron-rich phase formed on the rolled surface increases the corrosion rate of Mg−0.1Zr and Mg−0.3Si alloys after hot rolling. The corrosion rate of AZ31 alloy increases significantly after equal channel extrusion due to the existence of high density of dislocations and twins [128].

During the plastic deformation process, recrystallization occurs to produce fine grains and the distribution of the second phase is changed. It is conducive to improving the corrosion resistance as result of a more uniform microstructure. The

dynamic recrystallization of Mg−4Li−1Ca alloy occurs during hot rolling, reducing the grain size from 100 to 5 μm. The fine and uniformly distributed Mg_2Ca phases increase the number of corrosion sites evenly so that the corrosion type changes from local corrosion to uniform corrosion, thus improving the corrosion resistance of the alloy in SBF [57]. The better corrosion resistance of as-extruded Mg−11Li−3Al−2Zn−1.5Nd−0.2Zr alloy [129] and Mg−9Li−3Al−1.6Y alloy [58] can be also attributed to the grain refinement and the uniform distribution of intermetallic phases. As for the grain refinement of Mg−Li alloy during deformation process, it is suggested that high-density dislocations accumulate near the second phase particles to form crystal nuclei. In the meantime, the second phase particles hinder the growth of the grains, so as to produce fine recrystallized grains, which reduces the energy storage and dislocation density of the alloy. Hot-rolled Mg−Li alloy generates strong basal texture parallel to the rolling surface, which reduces the corrosion rate of the alloy. XIANG et al [65] studied the microstructures and corrosion properties of LA51 plates with different rolling reductions (0, 5%, 10%, 15% and 20%). The crystal plane of more grains parallel to the rolling surface is closer to the (0001) base plane when the reduction is 5% and 10%, leading to higher corrosion resistance. When the rolling reduction is 15% and 20%, the corrosion resistance of the alloy is improved because more $(10\bar{1}2)$ extension twins are generated, which accelerates the formation of surface oxide film and increases the charge transfer resistance. After cross-cold rolling of Mg−Li−Ca, dense and uniform corrosion products are formed on the surface, which significantly reduces the corrosion rate [59].

However, the plastic deformation can also introduce a large number of dislocations and strains in Mg−Li alloys, where corrosion damage easily happens. It has been found that the exfoliation corrosion occurred in the cold-rolled Mg−14Li−1Al [130], cold-rolled Mg−14Li−3Al [131], extruded Mg−Li−Ca [132] and ECAP Mg−14Li−1Al alloys [63]. The Mg−Li alloy possesses flat and slend grains along the rolling surface during the cold rolling process. Once the as-rolled alloy suffers pitting corrosion after the rupture of oxide film in the corrosive solution, the corrosion expands along the grain boundary and produces micro cracks, resulting in delamination along the rolling plane, that is, exfoliation corrosion. The exfoliation corrosion becomes more obvious when the rolling reduction increases, while the existence of equiaxial grains delays the initiation of cracks [131]. After annealing, the elongated grains are transformed into uniform equiaxial grains, so exfoliation corrosion is suppressed. DING et al [63] elaborated on the exfoliation corrosion mechanism of the extruded Mg−1Li−1Ca alloy, and concluded that the exfoliation corrosion of the extruded alloy is a synergistic effect of pitting, filamentous corrosion, intergranular corrosion and stress corrosion. As shown in Fig. 12 [63], firstly, the differences of grain size and stress distribution between the outer and inner layers promote the galvanic corrosion, then the galvanic corrosion of Mg_2Ca/Mg occurs. As the corrosion develops along the filiform trace, corrosion products, such as magnesium hydroxide, calcium hydroxide and lithium carbonate, are accumulated in the cracks, resulting in a wedge effect. Therefore, the exfoliation corrosion of extruded Mg−Li−Ca alloy starts at the Mg_2Ca particles and propagates along the extrusion direction or partly along the grain boundaries. In addition, as the rolling ratio increases from 3 to 10, the α-Mg phase is elongated and broken, which increases the amount of α-Mg/β-Li interfaces [19]. When the rolling ratio is 10, there are more micro couples and the area fraction of β-Li phase increases, leading to decreased corrosion resistance.

4.3 Heat treatment

Heat treatment can significantly affect the corrosion type and corrosion rate. Generally, heat treatment can accelerate the diffusion of atoms in the alloy, promote the dissolution or precipitation of the second phase, and cause changes in stress. Heat treatment in Mg alloys generally affects the corrosion rate of the alloy by changing the number and distribution of the second phase. When the second phase dissolves in the matrix or forms a continuous network corrosion barrier after solution treatment, the corrosion will be delayed. However, the precipitation of iron-rich cathodic phase by heat treatment can significantly increase the corrosion rate of the alloy. LIU et al [133] transformed the β-$(Mg,Zn)_3Gd$ eutectic phase in the as-cast Mg−15Gd−2Zn−0.39 Zr alloy into a LPSO phase by

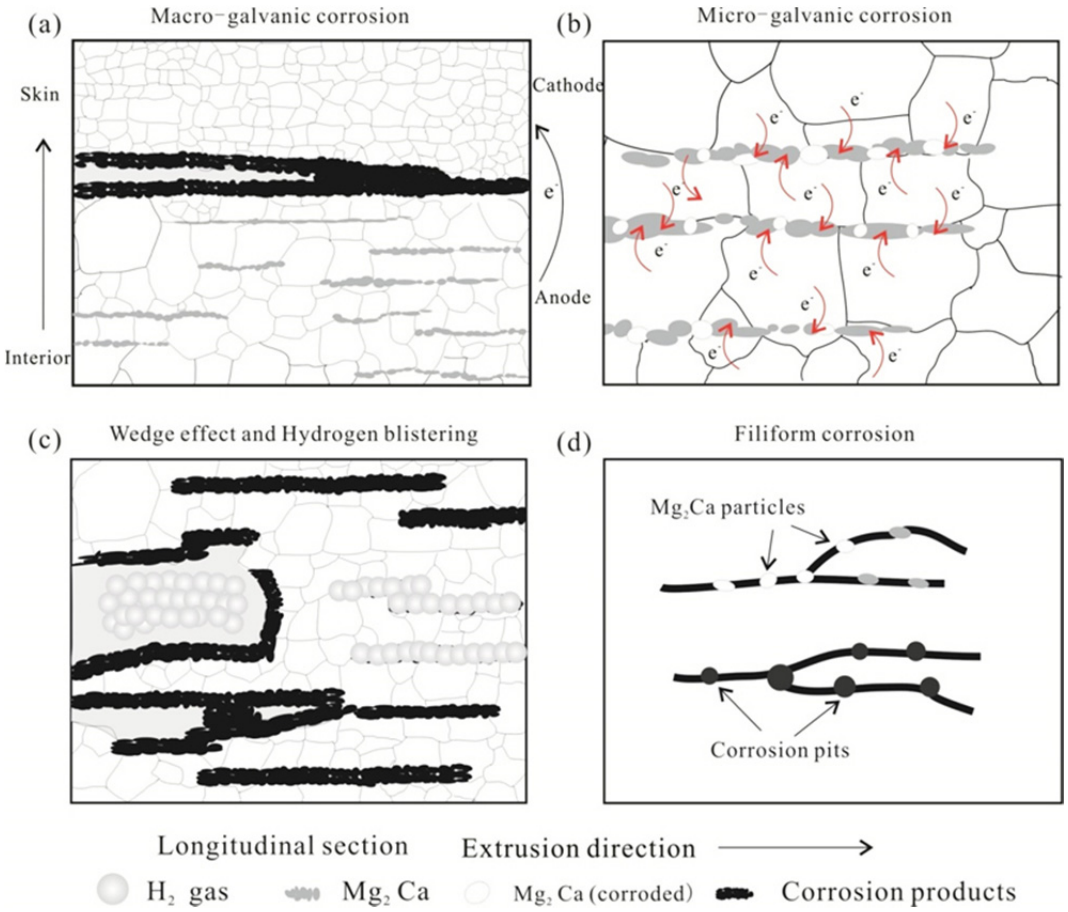

Fig. 12 Schematic illustration of exfoliation corrosion mechanism: (a) Macro-galvanic corrosion between skin layer and interior zone; (b) Micro-galvanic corrosion between Mg_2Ca and α-Mg; (c) Wedge effect and hydrogen blistering during exfoliation corrosion; (d) Pitting corrosion and filiform corrosion [63]

solid solution and aging. Because the local potential and volume fraction of the LPSO phase are significantly lower than those of the eutectic phase, the micro-galvanic corrosion between the second phase and the matrix is obviously reduced.

In Mg−Li alloy, solution, aging and annealing after deformation can significantly affect the corrosion behavior of the alloy. When Mg−8Li−4Y−2Er−2Zn−0.6Zr alloy is treated at 450 °C for 6 h, the fishbone-like second phase at the grain boundary and the granular second phase within the grains disappear, and the block-shaped second phases form [134]. In Mg−Li−Al alloys, solution treatment can promote the dissolution of AlLi phase and increase the content of Al in the matrix. During aging, $MgLi_2Al$ firstly precipitates from the matrix and then easily decomposes into AlLi and β-Li phases [135]. With the increase of aging time and temperature, the number of AlLi phase increases. As for the as-cast Mg−9Li alloy, after it is heated at 575 °C for 4.5 h, and then rapidly immersed in ice water mixture for quenching, due to the rapid bcc/hcp phase transition, the original bulk phase is completely transformed into fine needle-like phases, which is evenly distributed in the matrix [83]. This kind of microstructure can promote the surface film formed on the β-Li phase to completely cover the entire surface of the alloy to mitigate corrosion. In addition, due to insufficient atom diffusion during solid solution, there is a small difference in elemental concentration and electrochemical activity between α-Mg phase and β-Li phase, which reduces the pitting corrosion sensitivity and improves the corrosion resistance of the alloy. YU et al [61] compared the corrosion behavior of Mg−9Li−3Al−2.5Sr alloys at different aging temperatures and stated that the alloys aged at 150 °C for 6 h have the highest corrosion resistance, mainly because the aging temperature promotes the Al_4Sr phase evenly distributing along the grain boundary, which hinders further damage of corrosion. The corrosion resistance of Mg−Li alloy

can be enhanced by short time annealing at low temperature after extrusion or rolling. After being annealed at 200 °C for 1 h, incomplete dynamic recrystallization occurs in the cold-rolled LZ91 sheet driven by the large deformation energy and thermal energy stored in cold rolling [136]. The refined grains and the stable microstructure make the least corrosion pits and the least corrosion current density. The corrosion resistance of as-extruded Mg−7.5Li−3Al−1Zn alloy can be improved by annealing treatment, mainly because Li atom diffuses more rapidly, leading to the relative content of α-Mg phase and β-Li phase changing [137,138]. When the volume of β-Li increases from 29% to 35%, the area ratio of the cathode to the anode for galvanic corrosion is reduced, thereby effectively reducing the corrosion current.

It can be concluded from the above discussion that the change of grain size through heat treatment has little effect on the corrosion resistance of Mg−Li alloy, so the effect of the second phase on the corrosion is mainly concerned. Dissolving harmful second phases through solid solution treatment, precipitating favorable second phases through aging, and reducing defects through annealing treatment are the main ways for improving corrosion resistance of Mg−Li alloys.

5 Summary and outlook

There have been a considerable number of researches on the corrosion and protection of Mg−Li alloy. The literature on the corrosion behavior and influencing factors of Mg−Li alloy allows us to understand the corrosion mechanism more comprehensively and see the existing problems more clearly. The summary and outlook mentioned above are as follows.

(1) The corrosion behavior of Mg−Li alloy mainly varies with the Li content in the alloy, rather than with the crystal structure of HCP or BCC. Therefore, in order to investigate different corrosion behaviors of Mg−Li alloy from those of traditional Mg alloys, the corrosion characteristics and mechanism of the Mg−Li alloy with high Li content should be selected for the study.

(2) From the analysis of grain size, orientation and second phase, it can be inferred that the influence of the second phase is dominant. Hence, the corrosion resistance can be improved by reducing the content of the second phase in cathode and optimizing the distribution of the second phase.

(3) The addition of Li changes the composition and structure of the surface film of the Mg−Li alloys. In addition to Li_2CO_3, the chemical stability of the oxide film affected by the rapidly diffused Li should also be considered.

(4) Fine and uniform microstructure obtained by alloying, deformation and heat treatment can not only promote uniform corrosion, but also promote the formation of surface film, thus improving the corrosion resistance.

(5) The initial corrosion of Mg−Li alloy is mainly affected by the microstructure, such as the grain, and the second phase. The surface film often influences the long time corrosion behavior and average corrosion rate. In addition, the microstructure also affects the formation and structure of the surface film.

(6) The use of modern electrochemical methods and in situ techniques is conducive to the study of corrosion behavior and mechanism in a real corrosion environment, which promotes a deeper and more detailed study of corrosion behavior.

Acknowledgments

The authors are grateful for the financial supports from the Natural Science Foundation of China (Nos. 51771060, 51871068, 51971071, 52011530025), the Domain Foundation of Equipment Advance Research of the 13th Five-year Plan, China (No. 61409220118), the National Key Research and Development Program, China (No. 2021YFE0103200), the Zhejiang Province Key Research and Development Program, China (No. 2021C01086), and the Open Foundation of Key Laboratory of Superlight Materials & Surface Technology of Ministry of Education, China (No. HEU10202104)

References

[1] TAMMAN G M, MASING G. Behavior of lithium, toward sodium, potassium, yin, cadmium and magnesium. [J]. Zeitschrift fur Anorganische and Allgemeine Chemie, 1960, 67: 197−198.

[2] SANSCHAGRIN A, TREMBLAY R, ANGERS R, DUBÉ D. Mechanical properties and microstructure of new magnesium−lithium base alloys [J]. Materials Science and

Engineering A, 1996, 220(1/2): 69−77.

[3] WU R, YAN Y, WANG G, MURR L E, HAN W, ZHANG Z, ZHANG M. Recent progress in magnesium−lithium alloys [J]. International Materials Reviews, 2015, 60(2): 65−100.

[4] ZHANG Cheng, WU Liang, ZHAO Zi-long, XIE Zhi-hui, HUANG Guang-sheng, LIU Lei, JIANG Bin, ATRENS A, PAN Fu-sheng. Effect of Li content on microstructure and mechanical property of Mg−*x*Li−3(Al−Si) alloys [J]. Transactions of Nonferrous Metals Society of China, 2019, 29(12): 2506−2513.

[5] ZHANG Xue-song, CHEN Yong-jun, HU Jun-ling. Recent advances in the development of aerospace materials [J]. Progress in Aerospace Sciences, 2018, 97: 22−34.

[6] FRANKEL G S. Ready for the road [J]. Nature Materials, 2015, 14(12): 1189−1190.

[7] CHEN Xiao-yang, ZHANG Yang, CONG Meng-qi, LU Ya-lin, LI Xiao-ping. Effect of Sn content on microstructure and tensile properties of as-cast and as-extruded Mg−8Li−3Al−(1,2,3)Sn alloys [J]. Transactions of Nonferrous Metals Society of China, 2020, 30(8): 2079−2089.

[8] DING Hong-bo, LIU Qiang, ZHOU Hai-tao, ZHOU Xiao, ATRENS Andrej. Effect of thermal-mechanical processing on microstructure and mechanical properties of duplex-phase Mg−8Li−3Al−0.4Y alloy [J]. Transactions of Nonferrous Metals Society of China, 2017, 27(12): 2587−2597.

[9] JI Qing, WANG Yang, WU Rui-zhi, WEI Zhen, MA Xiao-chun, ZHANG Jing-huai, HOU Le-gan, ZHANG Mi-lin. High specific strength Mg−Li−Zn−Er alloy processed by multi deformation processes [J]. Materials Characterization, 2020, 160: 110135.

[10] ZHONG Feng, WU Hua-jie, JIAO Yun-lei, WU Rui-zhi, ZHANG Jing-huai, HOU Le-gan, ZHANG Mi-lin. Effect of Y and Ce on the microstructure, mechanical properties and anisotropy of as-rolled Mg−8Li−1Al alloy [J]. Journal of Materials Science & Technology, 2020, 39: 124−134.

[11] WANG Jia-hao, LI Yang, WU Rui-zhi, XU Lin, ZHANG Zhen, FENG Jing, ZHANG Jing-huai, HOU Le-gan, JIAO Yun-lei. X-band shielding properties of Mg−9Li matrix composite containing $Ni_{0.4}Zn_{0.4}Co_{0.2}Fe_2O_4$ fabricated by multi-layer composite rolling [J]. Journal of Alloys and Compounds, 2020, 843: 156053.

[12] WANG Jia-hao, XU Lin, WU Rui-zhi, FENG Jing, ZHANG Jing-huai, HOU Le-gan, ZHANG Mi-lin. Enhanced electromagnetic interference shielding in a duplex-phase Mg−9Li−3Al−1Zn alloy processed by accumulative roll bonding [J]. Acta Metallurgica Sinica (English Letters), 2020, 33(4): 490−499.

[13] WANG Dan, WU Hua-jie, WU Rui-zhi, WANG Yang, ZHANG Jing-huai, BETSOFEN S, KRIT B, HOU Le-gan, NODIR T. The transformation of LPSO type in Mg−4Y−2Er−2Zn−0.6Zr and its response to the mechanical properties and damping capacities [J]. Journal of Magnesium and Alloys, 2020, 8(3): 793−798.

[14] LIU Yang, WU Yuan-hao, BIAN Dong, GAO Shuang, LEEFLANG S, GUO Hui, ZHENG Yu-feng, ZHOU Jie. Study on the Mg−Li−Zn ternary alloy system with improved mechanical properties, good degradation performance and different responses to cells [J]. Acta Biomaterialia, 2017, 62: 418−433.

[15] JIN Si-yuan, LIU Hong-yu, WU Rui-zhi, ZHONG Feng, HOU Le-gan, ZHANG Jing-huai. Combination effects of Yb addition and cryogenic-rolling on microstructure and mechanical properties of LA141 alloy [J]. Materials Science and Engineering A, 2020, 788: 139611.

[16] SUN Yue-hua, WANG Ri-chu, PENG Chao-qun, FENG Yan, YANG Ming. Recent progress in Mg−Li matrix composites [J]. Transactions of Nonferrous Metals Society of China, 2019, 29(1): 1−14.

[17] GAO Gui-jia, ZENG Mei-qi, ZHANG En-liang, ZENG Rong-chang, CUI Lan-yue, XU Dao-kui, WANG Feng-qin, KANNAN M B. Dealloying corrosion of anodic and nano-metric $Mg_{41}Nd_5$ in solid solution-treated Mg−3Nd−1Li−0.2Zn alloy [J]. Journal of Materials Science & Technology, 2021, 83: 161−178.

[18] LI C Q, LIU X, DONG L J, SHI B Q, TANG S, DONG Y, ZHANG Z R. Simultaneously improved mechanical strength and corrosion resistance of Mg−Li−Al alloy by solid solution treatment [J]. Materials Letters, 2021, 301: 130305.

[19] WANG B J, XU D K, CAI X, QIAO Y X, SHENG L Y. Effect of rolling ratios on the microstructural evolution and corrosion performance of an as-rolled Mg−8 wt.%Li alloy [J]. Journal of Magnesium and Alloys, 2021, 9(2): 560−568.

[20] LUO Hong-jie, SONG Bin-na, LIU Yi-han, YAO Guang-chun. Electroless Ni−P plating on Mg−Li alloy by two-step method [J]. Transactions of Nonferrous Metals Society of China, 2011, 21(10): 2225−2230.

[21] YU Chi, CUI Lan-yue, ZHOU Yong-feng, HAN Zhuang-zhuang, CHEN Xiao-bo, ZENG Rong-chang, ZOU Yu-hong, LI Shuo-qi, ZHANG Fen, HAN En-hou, GUAN Shao-kang. Self-degradation of micro-arc oxidation/chitosan composite coating on Mg−4Li−1Ca alloy [J]. Surface and Coatings Technology, 2018, 344: 1−11.

[22] WEN Xin, CUI Xiu-fang, JIN Guo, JIAO Yun-lei, FANG Yong-chao. A novel Ni2MnCuSnAl0.1 multi-principal element alloy coating to enhance the wear resistance and corrosion resistance of Mg−Li alloy [J]. Optics & Laser Technology, 2021, 142: 107243.

[23] SUN Yue-hua, WANG Ri-chu, PENG Chao-qun, FENG Yan, YANG Ming. Corrosion behavior and surface treatment of superlight Mg−Li alloys [J]. Transactions of Nonferrous Metals Society of China, 2017, 27(7): 1455−1475.

[24] WANG Bao-jie, LUAN Ji-yu, XU Dao-kui, SUN Jie, LI Chuan-qiang, HAN En-hou. Research progress on the corrosion behavior of magnesium−lithium-based alloys: A Review [J]. Acta Metallurgica Sinica (English Letters), 2019, 32(1): 1−9.

[25] CAIN T W, LABUKAS J P. The development of β phase Mg−Li alloys for ultralight corrosion resistant applications [J]. npj Materials Degradation, 2020, 4(1): 1−10.

[26] WITTE F, KAESE V, HAFERKAMP H, SWITZER E, MEYER-LINDENBERG A, WIRTH C J, WINDHAGEN H. In vivo corrosion of four magnesium alloys and the associated bone response [J]. Biomaterials, 2005, 26(17): 3557−3563.

[27] SONG Ying-wei, SHAN Da-yong, CHEN Rong-shi, HAN En-hou. Corrosion characterization of Mg−8Li alloy in NaCl solution [J]. Corrosion Science, 2009, 51(5): 1087−1094.

[28] HUANG Ju-feng, SONG Guang-ling, ATRENS A,

DARGUSCH M. What activates the Mg surface — A comparison of Mg dissolution mechanisms [J]. Journal of Materials Science & Technology, 2020, 57: 204−220.

[29] HUANG X M, ZHANG C H, ZHANG M L. Corrosion behavior of pure Mg and Mg−Li Alloy in 3.5% NaCl of pH=7 [J]. Journal of Aeronautical Materials, 2008, 28(3): 71−76.

[30] SONG Y W, SHAN D Y, CHEN R S, HAN E H. Corrosion resistance of Mg−8.8Li alloy compared with AZ91 [J]. Corrosion Engineering, Science and Technology, 2011, 46(6): 719−723.

[31] DONG Lin-jie, LIU Xi, LIANG Jie-xi, LI Chuan-qiang, DONG Yong, ZHANG Zheng-rong. Corrosion behavior of a eutectic Mg−8Li alloy in NaCl solution [J]. Electrochemistry Communications, 2021, 129: 107087.

[32] XU W Q, BIRBILIS N, SHA G, WANG Y, DANIELS J E, XIAO Y, FERRY M. A high-specific-strength and corrosion-resistant magnesium alloy [J]. Nature Materials, 2015, 14(12): 1229−1235.

[33] YAN Y M, MALTSEVA A, ZHOU P, LI X J, ZENG Z R, GHARBI O, OGLE K, LA HAYE M, VAUDESCAL M, ESMAILY M, BIRBILIS N, VOLOVITCH P. On the in-situ aqueous stability of an Mg−Li−(Al−Y−Zr) alloy: Role of Li [J]. Corrosion Science, 2020, 164: 108342.

[34] QU Zhi-kun, WU Rui-zhi, ZHANG Jing-huai, ZHANG Mi-lin. Microstructures and corrosion resistance of three typical superlight Mg−Li alloys [J]. International Journal of Materials Research, 2014, 105(1): 58−64.

[35] CUI Lan-yue, SUN Lu, ZENG Rong-chang, ZHENG Yu-feng, LI Shuo-qi. In vitro degradation and biocompatibility of Mg−Li−Ca alloys—The influence of Li content [J]. Science China Materials, 2018, 61(4): 607−618.

[36] WU Jing-yao, ZHAO Dao-li, OHODNICKI J M, LEE B, ROY A, YAO R, CHEN S, DONG Zhong-yun, HEINEMAN W R, KUMTA P N. In vitro and in vivo evaluation of multiphase ultrahigh ductility Mg−Li−Zn alloys for cardiovascular stent application [J]. ACS Biomaterials Science & Engineering, 2018, 4(3): 919−932.

[37] ZONG Xi-mei, ZHANG Jin-shan, LIU Wei, CHEN Jin-gai, NIE Kai-bo, XU Chun-xiang. Effects of Li on microstructures, mechanical, and biocorrosion properties of biodegradable $Mg_{94-x}Zn_2Y_4Li_x$ alloys with long period stacking ordered phase [J]. Advanced Engineering Materials, 2017, 19(3): 1600606.

[38] LI C Q, XU D K, CHEN X B, WANG B J, WU R Z, HAN E H, BIRBILIS N. Composition and microstructure dependent corrosion behaviour of Mg−Li alloys [J]. Electrochimica Acta, 2018, 260: 55−64.

[39] LIU Xuan, LIU Shi-zhe, XUE Ji-lai. Discharge performance of the magnesium anodes with different phase constitutions for Mg-air batteries [J]. Journal of Power Sources, 2018, 396: 667−674.

[40] WANG Ri-chu, LI Qi, WANG Nai-guang, PENG Chao-qun, FENG Yan. Effect of lithium on the discharge and corrosion behavior of Mg−3wt.%Al alloy as the anode for seawater activated battery [J]. Journal of Materials Engineering and Performance, 2018, 27(12): 6552−6563.

[41] ZHAO Z L, LIU Y D, ZHONG Y F, CHEN X H, ZHANG Z Q. Corrosion resistance of as-rolled Mg−Li−AlSi alloys [J]. International Journal of Electrochemical Science, 2018, 13(5): 4338−4349.

[42] LI Chuan-qiang, HE Yi-bin, HUANG Huai-pei. Effect of lithium content on the mechanical and corrosion behaviors of HCP binary Mg−Li alloys [J]. Journal of Magnesium and Alloys, 2021, 9(2): 569−580.

[43] SUN Yue-hua, WANG Ri-chu, PENG Chao-qun, CAI Zhi-yong. Microstructure and corrosion behavior of as-extruded Mg−xLi−3Al−2Zn−0.2Zr alloys (x= 5, 8, 11 wt.%) [J]. Corrosion Science, 2020, 167: 108487.

[44] SUN Yue-hua, WANG Ri-chu, PENG Chao-qun, WANG Xiao-feng. Microstructure and corrosion behavior of as-homogenized Mg−xLi−3Al−2Zn−0.2Zr alloys (x=5, 8, 11 wt.%) [J]. Materials Characterization, 2020, 159: 110031.

[45] PRZONDZIONO J, WALKE W, HADASIK E, LALIK S. Potentiodynamic tests of magnesium alloy AZ31 with lithium additive [J]. Solid State Phenomena, 2013, 211: 93−100.

[46] LI C Q, XU D K, ZHANG Z R, HAN E H. Influence of the lithium content on the negative difference effect of Mg−Li alloys [J]. Journal of Materials Science & Technology, 2020, 57: 138−145.

[47] LIU Xuan, XUE Ji-lai, LIU Shi-zhe. Discharge and corrosion behaviors of the α-Mg and β-Li based Mg alloys for Mg−air batteries at different current densities [J]. Materials & Design, 2018, 160: 138−146.

[48] ATRENS A, SONG Guang-ling, LIU Ming, SHI Zhi-ming, CAO Fu-yong, DARGUSCH M S. Review of recent developments in the field of magnesium corrosion [J]. Advanced Engineering Materials, 2015, 17(4): 400−453.

[49] RALSTON K D, BIRBILIS N, DAVIES C H J. Revealing the relationship between grain size and corrosion rate of metals [J]. Scripta Materialia, 2010, 63(12): 1201−1204.

[50] OP′T HOOG C, BIRBILIS N, ESTRIN Y. Corrosion of pure Mg as a function of grain size and processing route [J]. Advanced Engineering Materials, 2008, 10(6): 579−582.

[51] WU Bao-liang, CHEN Bing, WANG Cheng-wei, JIAO Jing-ye, SHEN Qi-chao, ZHOU Tie-tao. Corrosion behavior of a novel Mg−13Li−X alloy with different grain sizes by rapid solidification rate [J]. Rare Metals, 2015, https://doi.org/10.1007/s12598-015-0601-7.

[52] YAO Lei, HAO Hai, JI Shou-hua, FANG Can-feng, ZHANG Xing-guo. Effects of ultrasonic vibration on solidification structure and properties of Mg−8Li−3Al alloy [J]. Transactions of Nonferrous Metals Society of China, 2011, 21(6): 1241−1246.

[53] MA Zhen-duo, PENG Qiang, WEI Guo-bing, YANG Yan, XU Tian-cai, XIE Wei-dong, LIU Gang, PENG Xiao-dong. Improvement of microstructure, mechanical property and corrosion resistance of Mg−9Li−3Al−1Ca alloy through centrifugal casting [J]. Metals and Materials International, 2021, 27(11): 4498−4509.

[54] LIU Gang, MA Zhen-duo, WEI Guo-bing, XU Tian-cai, ZHANG Xi, YANG Yan, XIE Wei-dong, PENG Xiao-dong. Microstructure, tensile properties and corrosion behavior of friction stir processed Mg−9Li−1Zn alloy [J]. Journal of Materials Processing Technology, 2019, 267: 393−402.

[55] SRIRAMAN N, KUMARAN S. Processing and understanding of light-weight Mg−4Li−xCa (0, 0.5 and 1)

alloy for bio-degradable implant applications [J]. Materials Today: Proceedings, 2020, 27: 1959−1961.

[56] GU M Y, WEI G L, LIU W C, WU G H. Influence of neodymium on microstructure and corrosion behavior of Mg−8Li−3Al−2Zn alloy [J]. Materials and Corrosion, 2017, 68(4): 436−443.

[57] NENE S S, KASHYAP B P, PRABHU N, ESTRIN Y, AL-SAMMAN T. Microstructure refinement and its effect on specific strength and bio-corrosion resistance in ultralight Mg−4Li−1Ca (LC41) alloy by hot rolling [J]. Journal of Alloys and Compounds, 2014, 615: 501−506.

[58] YANG Hao-miao, ZHANG Nan-yi, LIU Na, XIE Wei-dong, PENG Xiao-dong. Microstructure, mechanical properties, and corrosion resistance of Mg−9Li−3Al−1.6Y alloy [J]. Rare Metals, 2014, 35(5): 374−379.

[59] DHAMODHARAN D, BHAGAT SINGH P, KUMARAN S. Effect of grain size and secondary particle refinement on corrosion behavior of cross-rolled Mg−Li−Ca alloy [J]. Transactions of the Indian Institute of Metals, 2019, 72(6): 1631−1634.

[60] ULLMANN B, REIFENRATH J, SEITZ J M, BORMANN D, MEYER-LINDENBERG A. Influence of the grain size on the in vivo degradation behaviour of the magnesium alloy LAE442 [J]. Journal of Engineering in Medicine, 2013, 227(3): 317−326.

[61] YU Yuan-qing, PENG Xiao-dong, YI Hong-yu, LIU Jun-wei. Influence of various heat treatment on corrosion resistance of as-extruded Mg−9Li−3Al−2.5Sr alloys [J]. Materials Science Forum, 2014, 788: 41−44.

[62] GOLLAPUDI S. Grain size distribution effects on the corrosion behaviour of materials [J]. Corrosion Science, 2012, 62: 90−94.

[63] DING Zi-you, CUI Lan-yue, ZENG Rong-chang, ZHAO Yan-bin, GUAN Shao-kang, XU Dao-kui, LIN Cun-guo. Exfoliation corrosion of extruded Mg−Li−Ca alloy [J]. Journal of Materials Science & Technology, 2018, 34(9): 1550−1557.

[64] SONG Guang-ling, MISHRA R, XU Zhen-qing. Crystallographic orientation and electrochemical activity of AZ31 Mg alloy [J]. Electrochemistry Communications, 2010, 12(8): 1009−1012.

[65] XIANG Qing, JIANG Bin, ZHANG Yu-xin, CHEN Xiao-bo, SONG Jiang-feng, XU Jun-yao, FANG Liang, PAN Fu-sheng. Effect of rolling-induced microstructure on corrosion behaviour of an as-extruded Mg−5Li−1Al alloy sheet [J]. Corrosion Science, 2017, 119: 14−22.

[66] BLAND L G, GUSIEVA K, SCULLY J R. Effect of crystallographic orientation on the corrosion of magnesium: Comparison of film forming and bare crystal facets using electrochemical impedance and Raman spectroscopy [J]. Electrochimica Acta, 2017, 227: 136−151.

[67] SONG Guang-ling, XU Zhen-qing. Crystal orientation and electrochemical corrosion of polycrystalline Mg [J]. Corrosion Science, 2012, 63: 100−112.

[68] HAGIHARA K, OKUBO M, YAMASAKI M, NAKANO T. Crystal-orientation-dependent corrosion behaviour of single crystals of a pure Mg and Mg−Al and Mg−Cu solid solutions [J]. Corrosion Science, 2016, 109: 68−85.

[69] ZHANG Cheng, WU Liang, ZHAO Zi-long, HUANG Guang-sheng, JIANG Bin, ATRENS A, PAN Fu-sheng. Effect of the Al−Si eutectic on the microstructure and corrosion behavior of the single-phase Mg alloy Mg−4Li [J]. Journal of Magnesium and Alloys, 2021, 9(4): 1339−1348.

[70] ZHANG Cheng, WU Liang, ZHAO Zi-long, HUANG Guang-sheng, JIANG Bin, ATRENS A, PAN Fu-sheng. Effect of Al on the microstructure, corrosion behavior and mechanical properties of Mg−4Li [J]. Anti-Corrosion Methods and Materials, 2020, 67(1): 31−37.

[71] YANG Hua-bao, WU Liang, JIANG Bin, LIU Wen-jun, SONG Jiang-feng, HUANG Guang-sheng, ZHANG Ding-fei, PAN Fu-sheng. Clarifying the roles of grain boundary and grain orientation on the corrosion and discharge processes of α-Mg based Mg−Li alloys for primary Mg−air batteries [J]. Journal of Materials Science & Technology, 2021, 62: 128−138.

[72] WANG Bao-jie, XU Kai, XU Dao-kui, CAI Xiang, QIAO Yan-xin, SHENG Li-yuan. Anisotropic corrosion behavior of hot-rolled Mg−8wt.%Li alloy [J]. Journal of Materials Science & Technology, 2020, 53: 102−111.

[73] LI C Q, XU D K, YU S, SHENG L Y, HAN E H. Effect of icosahedral phase on crystallographic texture and mechanical anisotropy of Mg−4%Li based alloys [J]. Journal of Materials Science & Technology, 2017, 33(5): 475−480.

[74] HE Jun-jie, JIANG Bin, XU Jun, ZHANG Jian-yue, YU Xiao-wen, LIU Bo, PAN Fu-sheng. Effect of texture symmetry on mechanical performance and corrosion resistance of magnesium alloy sheet [J]. Journal of Alloys and Compounds, 2017, 723: 213−224.

[75] ZOU Guo-dong, PENG Qiu-ming, WANG Ya-nan, LIU Bao-zhong. The effect of extension twinning on the electrochemical corrosion properties of Mg−Y alloys [J]. Journal of Alloys and Compounds, 2015, 618: 44−48.

[76] WANG B J, XU D K, DONG J H, KE W. Effect of the crystallographic orientation and twinning on the corrosion resistance of an as-extruded Mg−3Al−1Zn (wt.%) bar [J]. Scripta Materialia, 2014, 88: 5−8.

[77] YANG Hua-bao, WU Liang, JIANG Bin, LEI Bin, LIU Wen-jun, SONG Jiang-feng, ATRENS A, HUANG Guang-sheng, ZHANG Ding-fei, PAN Fu-sheng. Enhancement of corrosion resistance and discharge performance of Mg−5Li−3Al−1Zn sheet for Mg−air battery via rolling [J]. Journal of the Electrochemical Society, 2020, 167(11): 110529.

[78] SONG G, ATRENS A. Understanding magnesium corrosion: A framework for improved alloy performance [J]. Advanced Engineering Materials, 2003, 5(12): 837−858.

[79] BAHMANI A, ARTHANARI S, SHIN K S. Formulation of corrosion rate of magnesium alloys using microstructural parameters [J]. Journal of Magnesium and Alloys, 2020, 8(1): 134−149.

[80] LIU Jin-hui, SONG Ying-wei, CHEN Jia-chen, CHEN Peng, SHAN Da-yong, HAN En-hou. The special role of anodic second phases in the micro-galvanic corrosion of EW75 Mg alloy [J]. Electrochimica Acta, 2016, 189: 190−195.

[81] SONG Ying-wei, SHAN Da-yong, HAN En-hou. Pitting corrosion of a rare earth Mg alloy GW93 [J]. Journal of Materials Science & Technology, 2017, 33(9): 954−960.

[82] AZZEDDINE H, HANNA A, DAKHOUCHE A, RABAHI L,

SCHARNAGL N, DOPITA M, BRISSET F, HELBERT A L, BAUDIN T. Impact of rare-earth elements on the corrosion performance of binary magnesium alloys [J]. Journal of Alloys and Compounds, 2020, 829: 154569.

[83] WANG Guo-wei, SONG Dan, LI Cheng, KLU E E, QIAO Yan-xin, SUN Jia-peng, JIANG Jing-hua, MA Ai-bin. Developing improved mechanical property and corrosion resistance of Mg−9Li alloy via solid-solution treatment [J]. Metals, 2019, 9(9): 920.

[84] MORISHIGE T, OBATA Y, GOTO T, FUKAGAWA T, NAKAMURA E, TAKENAKA T. Effect of Al composition on the corrosion resistance of Mg−14mass%Li system alloy [J]. Materials Transactions, 2016, 57(10): 1853−1856.

[85] PENG Xiang, XU Shi-hao, DING De-hua, LIAO Guang-lan, WU Guo-hua, LIU Wen-cai, DING Wen-jiang. Microstructural evolution, mechanical properties and corrosion behavior of as-cast Mg−5Li−3Al−2Zn alloy with different Sn and Y addition [J]. Journal of Materials Science & Technology, 2021, 72: 16−22.

[86] GU M, WEI G, ZHAO J, LIU W, WU G. Influence of yttrium addition on the corrosion behaviour of as-cast Mg−8Li−3Al−2Zn alloy [J]. Materials Science and Technology, 2017, 33(7): 864−869.

[87] DINESH P, MANIVANNAN S, KUMARESH BABU S P, NATARAJAN S. Effect of Nd on the microstructure and corrosion behaviour of Mg−9Li−3Al magnesium alloy in 3.5 wt.% NaCl solution [J]. Materials Today: Proceedings, 2019, 15: 126−131.

[88] XU D K, HAN E H. Effect of quasicrystalline phase on improving the corrosion resistance of a duplex structured Mg−Li alloy [J]. Scripta Materialia, 2014, 71: 21−24.

[89] LI Jin-guang, YANG Yan, DENG Hong-ju, LI Min-min, SU Jun-fei, HU Fa-ping, XIONG Xiao-ming, PENG Xiao-dong. Microstructure and corrosion behavior of as-extruded Mg−6.5Li−*x*Y−*y*Zn alloys [J]. Journal of Alloys and Compounds, 2020, 823: 153839.

[90] HU Zhi, YIN Zheng, YIN Zhou, WANG Kun, LIU Qi-dong, SUN Peng-fei, YAN Hong, SONG Hong-gun, LUO Chao, GUAN Hong-yu, LUC C. Corrosion behavior characterization of as extruded Mg−8Li−3Al alloy with minor alloying elements (Gd, Sn and Cu) by scanning Kelvin probe force microscopy [J]. Corrosion Science, 2020, 176: 108923.

[91] KWON J, BAEK S M, JUNG H, KIM J C, LEE S Y, PARK S S. Role of microalloyed Sm in enhancing the corrosion resistance of hot-rolled Mg−8Sn−1Al−1Zn alloy [J]. Corrosion Science, 2021, 185: 109425.

[92] ZENG Rong-chang, QI Wei-chen, ZHANG Fen, CUI Hong-zhi, ZHENG Yu-feng. In vitro corrosion of Mg−1.21Li−1.12Ca−1Y alloy [J]. Progress in Natural Science: Materials International, 2014, 24(5): 492−499.

[93] TAHERI M, PHILLIPS R C, KISH J R, BOTTON G A. Analysis of the surface film formed on Mg by exposure to water using a FIB cross-section and STEM-EDS [J]. Corrosion Science, 2012, 59: 222−228.

[94] NORDLIEN J H, NIŞANCIOĞU K, ONO S, MASUKO N. Morphology and structure of oxide films formed on MgAl alloys by exposure to air and water [J]. Journal of the Electrochemical Society, 1996, 143(8): 2564−2572.

[95] LI Chuan-qiang, TONG Zhi-pei, HE Yi-bin, HUANG Huai-pei, DONG Yong, ZHANG Peng. Comparison on corrosion resistance and surface film of pure Mg and Mg−14Li alloy [J]. Transactions of Nonferrous Metals Society of China, 2020, 30(9): 2413−2423.

[96] TANG Song, XIN Tong-zheng, XU Wan-qiang, MISKOVIC D, LI Chuan-qiang, BIRBILIS N, FERRY M. The composition-dependent oxidation film formation in Mg−Li−Al alloys [J]. Corrosion Science, 2021, 187: 109508.

[97] SONG Ying-wei, SHAN Da-yong, CHEN Rong-shi, HAN En-hou. Investigation of surface oxide film on magnesium lithium alloy [J]. Journal of Alloys and Compounds, 2009, 484(1/2): 585−590.

[98] ZENG Rong-chang, SUN Lu, ZHENG Yu-feng, CUI Hong-zhi, HAN En-hou. Corrosion and characterisation of dual phase Mg−Li−Ca alloy in Hank's solution: The influence of microstructural features [J]. Corrosion Science, 2014, 79: 69−82.

[99] KUMAR V. Detection and distribution of lithium in Mg−Li−Al based alloy by ToF-SIMS [J]. Applied Surface Science, 2016, 388: 64−70.

[100] LELEU S, RIVES B, BOUR J, CAUSSE N, PÉBÈRE N. On the stability of the oxides film formed on a magnesium alloy containing rare-earth elements [J]. Electrochimica Acta, 2018, 290: 586−594.

[101] CHEN Zi-han, BAO Chong-gao, WU Guo-qing, JIAN Yong-xin, ZHANG Li. Effect of YAl_2 particles on the corrosion behavior of Mg−Li matrix composite in NaCl solution [J]. Materials, 2019, 12(3): 549.

[102] XU Chun-hua, GAO Wei. Pilling−Bedworth ratio for oxidation of alloys [J]. Materials Research Innovations, 2000, 3(4): 231−235.

[103] HOU Li-feng, RAVEGGI M, CHEN Xiao-bo, XU Wan-qiang, LAWS K J, WEI Ying-hui, FERRY M, BIRBILIS N. Investigating the passivity and dissolution of a corrosion resistant Mg−33at.%Li alloy in aqueous chloride using online ICP-MS [J]. Journal of the Electrochemical Society, 2016, 163(6): C324−C329.

[104] YAN Y, QIU Y, GHARBI O, BIRBILIS N, NAKASHIMA P N H. Characterisation of Li in the surface film of a corrosion resistant Mg−Li(−Al−Y−Zr) alloy [J]. Applied Surface Science, 2019, 494: 1066−1071.

[105] YAN Y M, GHARBI O, MALTSEVA A, CHEN X B, ZENG Z R, XU S W, XU W Q, VOLOVICH P, FERRY M, BIRBILIS N. Investigating the structure of the surface film on a corrosion resistant Mg−Li(−Al−Y−Zr) alloy [J]. Corrosion, 2019, 75(1): 80−89.

[106] WANG Wen-hui, WU Hong-liu, SUN Yu, YAN Jun, ZHANG Lei, ZHANG Shao-xiang, NI Jia-hua, SONG Yang, ZHANG Xiao-nong. Local intragranular misorientation accelerates corrosion in biodegradable Mg [J]. Acta Biomaterialia, 2020, 101: 575−585.

[107] VAUGHAN M W, KARAYAN A I, SRIVASTAVA A, MANSOOR B, SEITZ J M, EIFLER R, KARAMAN I, CASTANEDA H, MAIER H J. The effects of severe plastic deformation on the mechanical and corrosion characteristics of a bioresorbable Mg-ZKQX6000 alloy [J]. Materials Science and Engineering: C, 2020, 115: 111130.

[108] JOHNSTON S, SHI Zhi-ming, ATRENS A. The influence of pH on the corrosion rate of high-purity Mg, AZ91 and ZE41 in bicarbonate buffered Hanks' solution [J]. Corrosion Science, 2015, 101: 182−192.

[109] ZHAO Zi-long, LI Yi-hao, ZHONG Yi-feng, LIU Yi-ding. Corrosion performance of as-rolled Mg−8Li−*x*Al alloys [J]. International Journal of Electrochemical Science, 2019, 14(7): 6394−6405.

[110] GAO Li-li, ZHANG Chun-hong, ZHANG Mi-lin, HUANG Xiao-mei, SHENG Nan. The corrosion of a novel Mg−11Li−3Al−0.5RE alloy in alkaline NaCl solution [J]. Journal of Alloys and Compounds, 2009, 468(1/2): 285−289.

[111] WITTE F, FISCHER J, NELLESEN J, CROSTACK H A, KAESE V, PISCH A, BECKMANN F, WINDHAGEN H. In vitro and in vivo corrosion measurements of magnesium alloys [J]. Biomaterials, 2006, 27(7): 1013−1018.

[112] MORISHIGE T, UENO K, OKANO M, GOTO T, NAKAMURA E, TAKENAKA T. Effect of impurity Fe concentration on the corrosion behavior of Mg−14mass%Li−1mass%Al alloy [J]. Materials Transactions, 2014, 55(9): 1506−1509.

[113] WU Jing-yao, ZHAO Dao-li, LEE B, ROY A, YAO R, CHEN S, DONG Zhong-yun, HEINEMAN W R, KUMTA P N. Effect of lithium and aluminum on the mechanical properties, in vivo and in vitro degradation, and toxicity of multiphase ultrahigh ductility Mg−Li−Al−Zn quaternary alloys for vascular stent application [J]. ACS Biomaterials Science & Engineering, 2020, 6(4): 1950−1964.

[114] ZHAO Zi-long, XING Xue-gang, LUO Li, WANG Yi-de, LIANG Wei. Influence of Al−Si additions on mechanical properties and corrosion resistance of Mg−8Li dual-phase alloys [J]. Journal of Iron and Steel Research International, 2017, 24: 426−429.

[115] LV Yan-zhuo, LIU Min, XU Yan, CAO Dian-xue, FENG Jing. The electrochemical behaviors of Mg−8Li−3Al−0.5Zn and Mg−8Li−3Al−1.0Zn in sodium chloride solution [J]. Journal of Power Sources, 2013, 225: 124−128.

[116] XIONG Xiao-ming, YANG Yan, DENG Hong-ju, LI Min-min, LI Jin-guang, WEI Guo-bing, PENG Xiao-dong. Effect of Ca content on the mechanical properties and corrosion behaviors of extruded Mg−7Li−3Al alloys [J]. Metals, 2019, 9(11): 1212.

[117] DONG Tian-shun, LI Xiao-bing, FU Bin-guo, LI Guo-lu, LIU Jin-hai. Influence of Ca on microstructure and corrosion resistance of Mg−14Li alloy [J]. China Foundry, 2018, 15(2): 132−138.

[118] LIU Ming, SCHMUTZ P, UGGOWITZER P J, SONG Guang-ling, ATRENS A. The influence of yttrium (Y) on the corrosion of Mg−Y binary alloys [J]. Corrosion Science, 2010, 52(11): 3687−3701.

[119] MANIVANNAN S, DINESH P, MAHEMAA R, MARIYAPILLAI N, KUMARESH BABU S P, SUNDARRAJAN S. Corrosion behavior of as-cast Mg−8Li−3Al−*x*Ce alloy in 3.5 wt.% NaCl solution [J]. International Journal of Minerals, Metallurgy, and Materials, 2016, 23(10): 1196−1203.

[120] LV Yan-zhuo, XU Yan, CAO Dian-xue. The electrochemical behaviors of Mg, Mg−Li−Al−Ce and Mg−Li−Al−Ce−Y in sodium chloride solution [J]. Journal of Power Sources, 2011, 196(20): 8809−8814.

[121] LV Yan-zhuo, LIU Min, XU Yan, CAO Dian-xue, FENG Jing, WU Rui-zhi, ZHANG Mi-lin. The electrochemical behaviors of Mg−8Li−0.5Y and Mg−8Li−1Y alloys in sodium chloride solution [J]. Journal of Power Sources, 2013, 239: 265−268.

[122] YU Ju-xin, LV Yan-zhuo, DUAN Ti-gang, MENG Fei, CHENG Qing, XU Yan, ZHOU Kai-wen, XUE Li-li, LENG Zhe. Discharge and corrosion behaviors of Mg−Li and Mg−Li−La alloys as anodes for seawater battery [J]. International Journal of Electrochemical Science, 2020: 10922−10935.

[123] ZHANG Jia-xin, ZHANG Jin-shan, HAN Fu-yin, LIU Wei, ZHANG Long-long, ZHAO Rui, XU Chun-xiang, DOU Jing. Modification of Mn on corrosion and mechanical behavior of biodegradable $Mg_{88}Y_4Zn_2Li_5$ alloy with long-period stacking ordered structure [J]. Journal of Materials Science & Technology, 2020, 42: 130−142.

[124] JEONG S H, KIM B J, LIM H K, KIM W T, KIM D H, JEON S H. Effect of Zr addition on the corrosion behavior of extruded Mg alloys in NaCl solution [J]. Materials Transactions, 2018, 59(3): 499−502.

[125] CAIN T W, LABUKAS J P. Magnesium technology 2020 [M]. Cham: Springer, 2020: 43−48.

[126] HE Yu-qing, PENG Chao-qun, FENG Yan, WANG Ri-chu, ZHONG Jian-feng. Effects of alloying elements on the microstructure and corrosion behavior of Mg−Li−Al−Y alloys [J]. Journal of Alloys and Compounds, 2020, 834: 154344.

[127] CAO Fu-yong, SHI Zhi-ming, SONG Guang-ling, LIU Ming, DARGUSCH M S, ATRENS A. Influence of hot rolling on the corrosion behavior of several Mg−X alloys [J]. Corrosion Science, 2015, 90: 176−191.

[128] HAMU G B, ELIEZER D, WAGNER L. The relation between severe plastic deformation microstructure and corrosion behavior of AZ31 magnesium alloy [J]. Journal of Alloys and Compounds, 2009, 468(1/2): 222−229.

[129] LEI Xue, WANG Ri-chu, PENG Chao-qun, FENG Yan, SUN Yue-hua. Effect of hot extrusion on the microstructure, mechanical properties, and corrosion behavior of Mg−11Li−3Al−2Zn−1.5Nd−0.2Zr alloy [J]. Transactions of the Indian Institute of Metals, 2019, 72(10): 2893−2899.

[130] MORISHIGE T, DOI H, GOTO T, NAKAMURA E, TAKENAKA T. Exfoliation corrosion behavior of cold-rolled Mg−14mass%Li−1mass%Al alloy in NaCl solution [J]. Materials Transactions, 2013, 54(9): 1863−1866.

[131] OBATA Y, MORISHIGE T, GOTO T, NAKAMURA E, TAKENAKA T. Relationship between microstructure and exfoliation corrosion in Mg−14mass%Li−3mass%Al cold-rolled alloy [J]. Materials Science Forum, 2018, 941: 1743−1747.

[132] IKOMA H, MORISHIGE T, TAKENAKA T. The influence of introduced strains on the exfoliation corrosion behavior of Mg−14mass%Li−1mass%Al alloy [J]. Materials Science Forum, 2021, 1016: 587−591.

[133] LIU Jing, YANG Li-xin, ZHANG Chun-yan, ZHANG Bo, ZHANG Tao, LI Yang, WU Kai-ming, WANG Fu-hui. Significantly improved corrosion resistance of Mg−15Gd−2Zn−0.39Zr alloys: Effect of heat-treatment [J]. Journal of

Materials Science & Technology, 2019, 35(8): 1644−1654.
[134] WANG Dan, LIU Shu-juan, WU Rui-zhi, ZHANG Shun, WANG Yang, WU Hua-jie, ZHANG Jing-huai, HOU Le-gan. Synergistically improved damping, elastic modulus and mechanical properties of rolled Mg−8Li−4Y−2Er−2Zn−0.6Zr alloy with twins and long-period stacking ordered phase [J]. Journal of Alloys and Compounds, 2021, 881: 160663.
[135] MAURYA R, MITTAL D, BALANI K. Effect of heat-treatment on microstructure, mechanical and tribological properties of Mg−Li−Al based alloy [J]. Journal of Materials Research and Technology, 2020, 9(3): 4749−4762.
[136] MA Li-na, YANG Yan, ZHOU Gang, REN Feng-juan, DENG Hong-ju, WEI Guo-bing, PENG Xiao-dong. Effect of rolling reduction and annealing process on microstructure and corrosion behavior of LZ91 alloy sheet [J]. Transactions of Nonferrous Metals Society of China, 2020, 30(7): 1816−1825.
[137] DOBKOWSKA A, ADAMCZYK-CIEŚLAK B, KUBÁSEK J, VOJTĚCH D, KUC D, HADASIK E, MIZERA J. Microstructure and corrosion resistance of a duplex structured Mg−7.5Li−3Al−1Zn [J]. Journal of Magnesium and Alloys, 2021, 9(2): 467−477.
[138] JIN Si-yuan, MA Xiao-chun, WU Rui-zhi, LI Ting-qu, WANG Jia-xiu, KRIT B L, HOU Le-gan, ZHANG Jing-huai, WANG Gui-xiang. Effect of carbonate additive on the microstructure and corrosion resistance of plasma electrolytic oxidation coating on Mg−9Li−3Al alloy [J]. International Journal of Mineral Metallurgy and Materials, 2021. https://doi.org/10.1007/s12613-021-2377-0.

镁锂合金腐蚀综述

马晓春[1]，靳思远[1]，巫瑞智[1,2]，王甲秀[1]，王桂香[1]，Boris KRIT[3]，Sergey BETSOFEN[3]

1. 哈尔滨工程大学 超轻材料与表面技术教育部重点实验室，哈尔滨 150001；
2. 黑河学院 理学院，黑河 164300；
3. Moscow Aviation Institute, National Research University, Moscow 125993, Russia

摘　要：镁锂合金耐蚀性差是制约其广泛应用的关键问题。本文在总结大量镁锂合金腐蚀行为研究的基础上，阐述镁锂合金腐蚀行为的影响因素和提高其耐蚀性的加工工艺。首先，介绍镁锂合金的腐蚀特点；然后，重点解释晶粒尺寸、晶粒取向、第二相和表面膜对腐蚀行为的影响规律，并通过合金化、塑性变形和热处理工艺改变镁锂合金腐蚀性能。进一步深入讨论镁锂合金的腐蚀机理；最后，提出针对提高镁锂合金耐蚀性应重点关注的方面。

关键词：镁锂合金；腐蚀行为；显微组织；表面膜；合金化；塑性变形；热处理

(Edited by Wei-ping CHEN)